

The Sawqirah contourite drift system in the Arabian Sea (NW Indian Ocean): A case study of interactions between margin reactivation and contouritic processes



M. Rodriguez ^{a,*}, J. Bourget ^b, N. Chamot-Rooke ^a, P. Huchon ^c, M. Fournier ^c, M. Delescluse ^a, S. Zaragosi ^d

^a Laboratoire de Géologie de l'Ecole normale supérieure de Paris, PSL Research University, CNRS UMR 8538, 24 rue Lhomond, 75005 Paris, France

^b Centre for Energy Geoscience, School of Earth and Environment, University of Western Australia, 35 Stirling Hwy, Crawley, WA 6009, Australia

^c Sorbonne Universités, UPMC Université Paris 6, CNRS, Institut des Sciences de la Terre Paris, 4 place Jussieu, 75005 Paris, France

^d EPOC Université de Bordeaux, UMR 5805, avenue des facultés, 33405 Talence, France

ARTICLE INFO

Article history:

Received 18 February 2016

Received in revised form 1 July 2016

Accepted 21 August 2016

Available online 24 August 2016

Keywords:

Contourite

Monsoon

Upwelling

Indian Ocean

Oman margin

Post-rift margin reactivation

Arabian Sea

ABSTRACT

The relationships between oceanic circulation in the Arabian Sea and Late Cenozoic climate changes, including variations in monsoon intensity at the million year time-scale, remain poorly investigated. Using multibeam and seismic data, we provide the first description of a contourite drift in the Arabian Sea, along the south-eastern Oman margin. This contourite drift is referred as the “Sawqirah Contourite Drift System”. Late Miocene reactivation of the south-eastern Oman margin resulted in the formation of a complex anticline system, which shaped the seafloor topography above which the Sawqirah Drift subsequently developed. The drift resulted from the circulation of bottom currents within the North Intermediate Indian Water. Major seismic unconformities identified within the Sawqirah Drift were tied to Ocean Drilling Program (ODP) drill holes, and allowed defining distinct episodes of drift construction. At least two of these unconformities record reorganizations of the oceanic circulation at ~4.5–4.8 Ma and ~2.4 Ma. The 4.5–4.8 Ma-old unconformity is coeval with the onset of upwelling of deep and cold waters in the Owen Basin. The 2.4 Ma-old unconformity records a major episode of Indian monsoon intensification (at the million year time scale) over the Arabian Sea, indicating strong coupling between oceanic and atmospheric circulation processes.

© 2016 Published by Elsevier B.V.

1. Introduction

The global oceanic circulation underwent several reorganization phases during the Late Cenozoic in response to plate tectonic events and climate-eustatic changes. In the Early Miocene, intermediate and deep-water masses in the Atlantic and Pacific Oceans all originated from water masses surrounding Antarctica, and aged towards the Arctic (Woodruff and Savin, 1989). Several tectonic events contributed to the development of the thermohaline circulation and the differentiation of the isotopic signature of water masses (Billups, 2002; Bickert et al., 2004; Poore et al., 2006): the closure of the Panama Strait beginning in the Middle Miocene (Montes et al., 2015), the opening of the Gibraltar Strait in the Central Atlantic at 5.3 Ma (Hernández-Molina et al., 2014), and the closure of the Indonesian Seaway in south-east Asia at ~3–4 Ma (Fig. 1; Cane and Molnar, 2001). The sea level drop-down induced by the onset of permanent ice-sheets in the northern hemisphere around 2.7 Ma (Bailey et al., 2013) also contributed to the emergence of the straits (Molnar, 2008; Miller et al., 2011).

Major changes in thermohaline circulation have strong effects on sedimentation. Currents generate deposits known as contourite drifts, and several types of erosive features forming contourite channels, moats or terraces. The architecture, distribution, and stratigraphy of contourite drift systems provide strong constraints on long term (10^5 – 10^6 years) intermediate and deep-sea circulation changes (Faugères et al., 1999; Rebesco et al., 2014). Since the onset of the thermohaline circulation, several continental margins experienced tectonic reactivation, expressed by inversion of rifted structures or gravity-driven tectonics that influenced the build-up of contourite drift systems (for instance in the Alboran Sea, Ercilla et al., 2016; Juan et al., 2016).

Contourite drifts are poorly documented along the Indian Ocean's margins (Rebesco et al., 2014). The best-studied area of contourite deposition is the Maldives carbonate platform (Betzler et al., 2013; Lüdmann et al., 2013). In the western Indian Ocean, a few preliminary studies also document contourites in the vicinity of the Amirante Ridge south to the Seychelles (Damuth and Johnson, 1989), in the Mozambique Basin (Preu et al., 2011), and off South Africa, where the Indian and the Atlantic oceans connect (Ben-Avraham et al., 1994; Niemi et al., 2000; Uenzelmann-Neben et al., 2011; Wiles et al., 2014; Gruetzner and Uenzelmann-Neben, 2016). Where available, stratigraphic constraints within these contourite drift systems document a Middle

* Corresponding author.

E-mail address: rodriguez@geologie.ens.fr (M. Rodriguez).

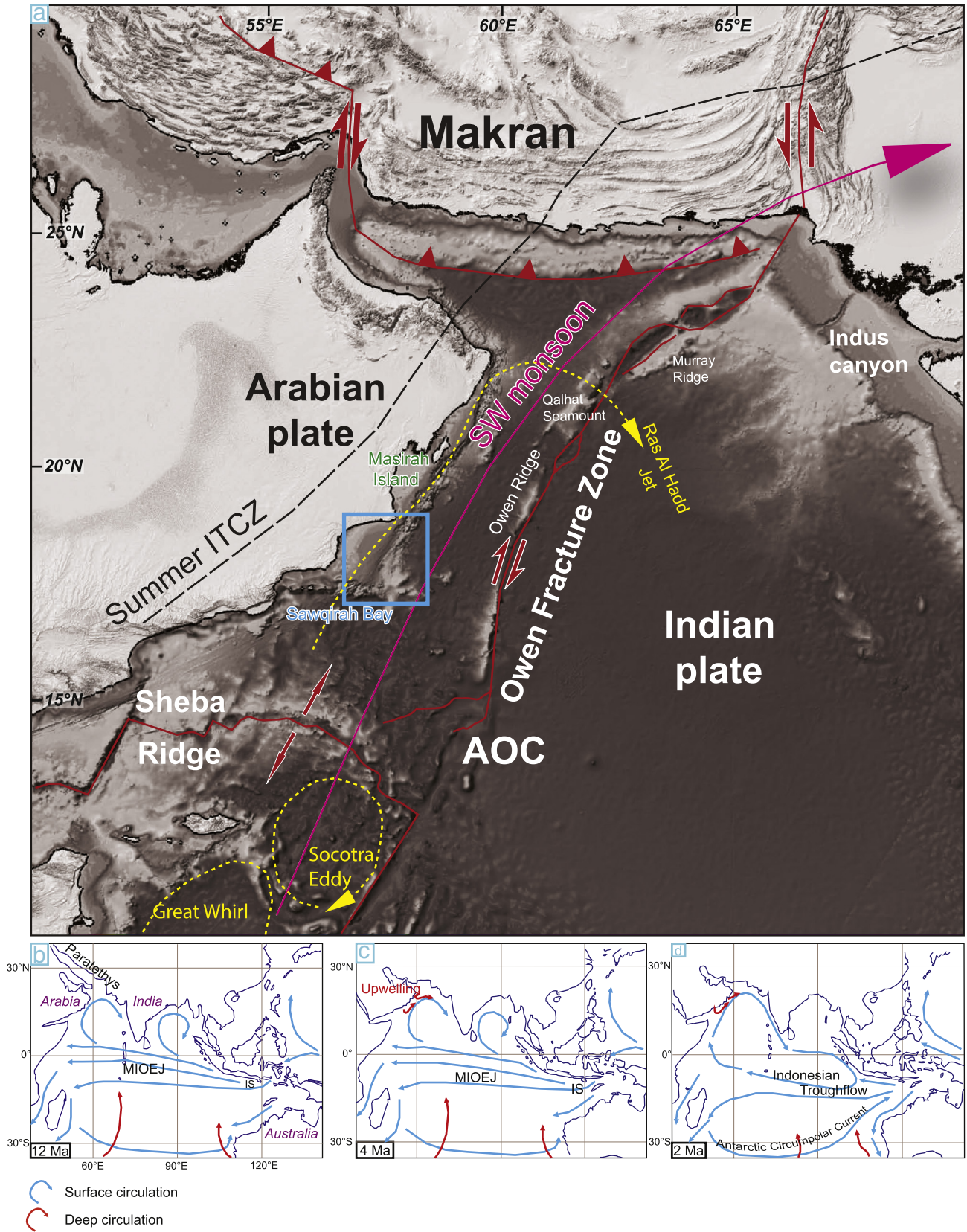


Fig. 1. a) Regional tectonic map of the Arabian Sea. The black dashed arrow represents the position of the summer Inter-Tropical Convergence Zone (ITCZ), and the yellow dotted line the path of the Ras Al Hadd Jet and other local surface currents (for the summer monsoon configuration; Schott and McCreary, 2001). The pink line represents the summer monsoon winds. AOC: Aden-Owen-Carlsberg triple junction, configuration according to Fournier et al., 2008. b) to d): schematic reconstructions of oceanic circulation in the Indian Ocean since Tortonian times, modified from Gourelan et al. (2008). Plate reconstructions are from Seton et al. (2012). For more detailed reconstructions of the present-day oceanic circulation, including its seasonal changes in response to fluctuations in the monsoon regime, see Schott and McCreary, 2001. MIOEJ: Miocene Indian Ocean Equatorial Jet, IS: Indonesian Seaway.

Miocene change in the oceanic circulation, following the closure of the Paratethys gateway between Arabia and Eurasia (Fig. 1; Preu et al., 2011). In the eastern Indian Ocean, a contourite drift is identified at the Sunda Arc (Sumba Drift, Reed et al., 1987), where connection with Pacific waters takes place. Contourite drifts are also suspected in the surroundings of the Bengal Fan (Kolla et al., 1976). Although contourite drifts may provide a valuable archive of the paleoceanographic changes

of the Indian Ocean in response to the various tectonic and climatic events that occurred during the Cenozoic (Allen and Armstrong, 2008; Gourelan et al., 2008; Butzin et al., 2011; Le Houedec et al., 2012), the seismic imaging of their architecture and the available stratigraphic constraints are scarce.

This study uses a new dataset composed of multibeam bathymetry data, high-resolution (3.5 kHz) echosounder data and 24 channels

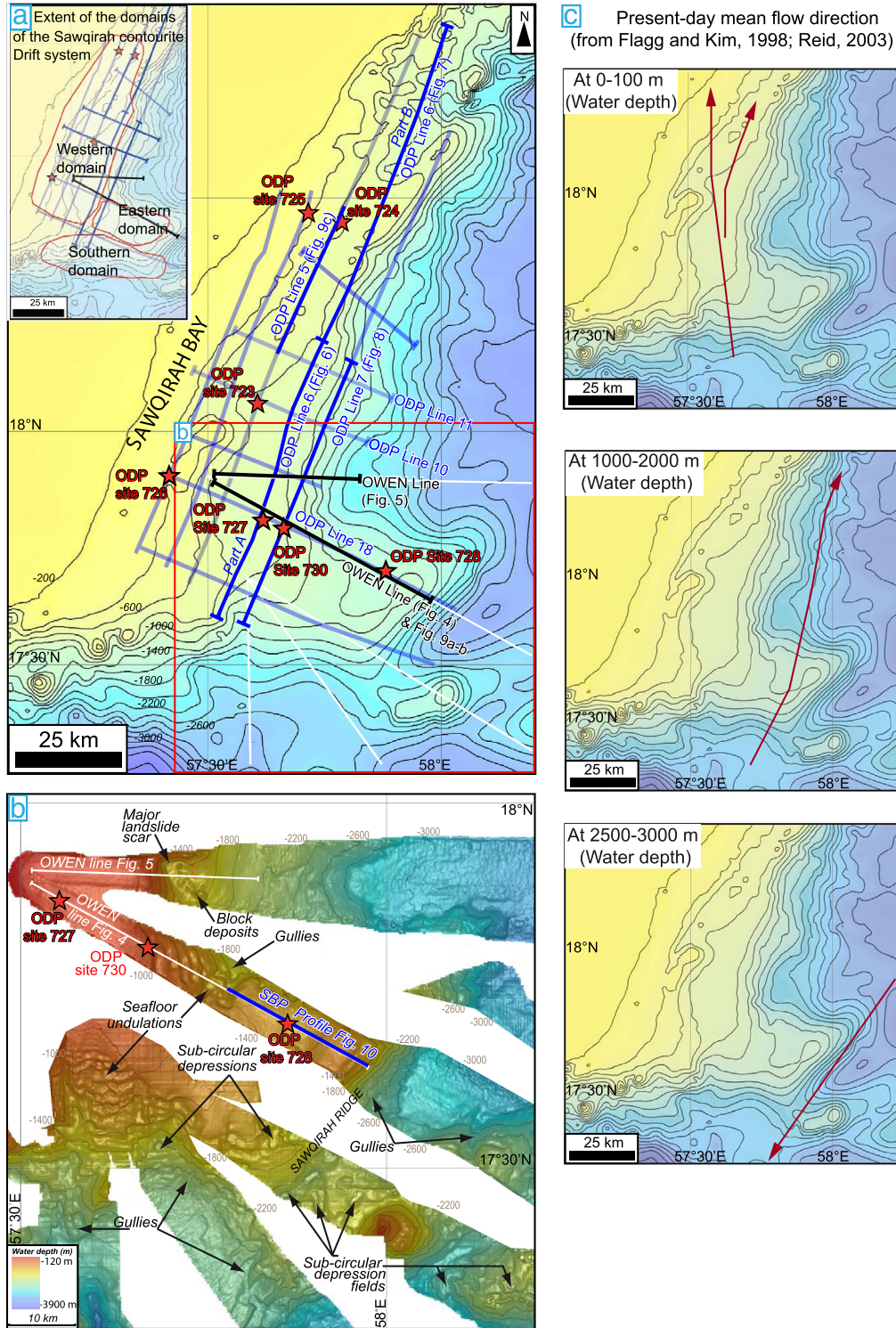


Fig. 2. a) Bathymetric map of the South East Oman margin and the Sawqirah Bay at 200 m contour interval, with location of ODP drilling sites, and ODP and OWEN seismic lines. Dark blue ODP Lines are the ones presented in this study. Inset shows the extent of the different domains of the Sawqirah anticline/drift, white lines indicate multibeam tracks; b) Partial multibeam covering of the Sawqirah Ridge, showing undulated seafloor morphology, as well as gullies and mass failures. c) Present-day mean flow direction of oceanic currents at various water depths (Flagg and Kim, 1998; Reid, 2003).

seismic data, as well as seismic data previously collected during the ODP Leg 117 (Shipboard Scientific Party, 1989) to describe Late Cenozoic contourite deposits along the South-East Oman margin (Figs. 1, 2). The South-East Oman margin experienced tectonic reactivation during the Late Miocene (Rodríguez et al., 2014a). It constitutes a good study area to investigate how interactions between contour currents and tectonics control the evolution of a contourite drift system. Stratigraphic data from Ocean Drilling Program (ODP) Sites calibrate the seismic stratigraphic analysis, and locally provide age constraints of the strata from the Middle Miocene onwards (Shipboard Scientific Party, 1989).

The main objectives of this study are 1) to describe the architecture of contourite deposits off South-East Oman and their interaction with local tectonics and gravity-driven, downslope sedimentary processes; 2) to understand how and where contourites accumulated in the tectonic context of the South-East Oman margin (Rodríguez et al., 2014a, 2014b); 3) to identify major seismic stratigraphic features (unconformities and drift-building sequences) indicative of changes in deep-sea circulation (i.e. intensity and pathway) or tectonics; and 4) to track the potential drivers of the circulation changes by investigating the multi-proxy record of the Indian monsoon intensity (Shipboard Scientific Party, 1989; Quade et al., 1989; Bloemendal et al., 1993; Clemens et al., 1996; Molnar, 2005; Huang et al., 2007; Clift et al., 2008; Sanyal and Sinha, 2010; Sanyal et al., 2010; Molnar et al., 2010; Zachos et al., 2001; Clift et al., 2014; Kroon et al., 1991).

2. Geological and oceanographic setting of the Owen Basin (Arabian Sea)

2.1. Geological background

The South-East Oman margin is a ~600-km-long, 5 to 10°-steep fossil transform margin (Mountain and Prell, 1990; Barton et al., 1990), which is dissected by turbidite systems (e.g. the Al Batha system; Bourget, 2009; Bourget et al., 2010). During the Paleogene, the India-Arabia plate boundary was running at the edge of the South-Eastern Oman margin (Rodríguez et al., 2016). The tectonic activity of the Paleogene India-Arabia boundary triggered the uplift of a system of marginal ridges, including the Sawqirah Ridge in South East Oman (Rodríguez et al., 2016). The plate-boundary jumped close its present-day location at the Owen Fracture Zone (Fournier et al., 2011; Rodríguez et al., 2011, 2014b) in response to a plate reorganization affecting the entire Indian Ocean during the Late Eocene-Oligocene (Rodríguez, 2013; Rodríguez et al., 2016). A Late Miocene tectonic episode, beginning at 8.2–8.8 Ma in response to a major plate reorganization event in the Indian Ocean (Merkouriev and DeMets, 2006; Delescluse et al., 2008; DeMets et al., 2015), affected the Owen Basin (Rodríguez et al., 2014a, 2014b). This episode of deformation reactivated the Oman transform margin, and triggered the uplift of the Owen Ridge. The Late Miocene reactivation of the Oman margin formed a large anticline system (or anticlinorium) in the area of the Sawqirah Bay between ~17°30' and 18°30'N (Fig. 2, Rodríguez et al., 2014a), which is hereafter referred as the "Sawqirah Anticline System".

2.2. Present-day oceanic circulation in the Arabian Sea

The Oman coast is currently swept by a northward strong surface current (with a velocity on the order of $1 \text{ m} \cdot \text{s}^{-1}$) referred as the Ras Al Hadd Jet (Fig. 1; Böhm et al., 1999; Shi et al., 1999, 2000). Despite seasonal variations at the scale of the Arabian Sea, the trend of the surface flow remains oriented SW-NE in the vicinity of the Sawqirah Anticline System (Fig. 2c; Shi et al., 2000). At intermediate depths (~200–1500 m), a combination of waters coming from the Somali Basin, the Persian Gulf, the Red Sea, and the Gulf of Aden forms the North Indian Intermediate Water (NIIW hereafter, Shipboard Scientific Party, 1989; You and Tomczak, 1993; Morrison, 1997; Beal et al., 2000; Al Saafani and Sheno, 2007), whose upper bound corresponds to the thermocline

(Figs. 2c, 3). The NIIW currently coincides in depth with the Oxygen Minimum Zone off Oman (Hermelin, 1992). Currents within the NIIW flow dominantly north-northeastwards at Sawqirah according to measurements performed in the 90's (Fig. 2c, Flagg and Kim, 1998). Velocities of currents are on the order of $5\text{--}10 \text{ cm} \cdot \text{s}^{-1}$ at 400 m water depth (Flagg and Kim, 1998), no measurement being available for deeper currents. At the Ras Al Hadd, currents within the NIIW deviate eastwards to the Qalhat Seamount and the Murray Ridge, and flow back southwards along the Owen Ridge (Reid, 2003). In the Arabian Sea, transient episodes of reversing of deep-water circulation occur in response to seasonal monsoon fluctuations, possibly through Rossby waves (Beal et al., 2000). Intermediate waters are upwelled between the coast and the area of the Sawqirah anticline (Shi et al., 2000; Schott et al., 2002). The upwelling is under the control of seasonal, fast monsoon winds (i.e. Findlater Jet; Böhm et al., 1999). Well-organized and coherent upwelling circulation is only sporadic and transient in the Arabian Sea (Muraleedharan and Kumar, 1996; Brink et al., 1998; You, 1997). During the winter monsoon, monsoon winds combined with Ekman pumping cause the downwelling of high-salinity surface waters east of the Owen Ridge, and their mixing with intermediate waters (Morrison, 1997; Schott et al., 2002). There is no formation of deep waters in the Arabian Sea (Morrison, 1998). Deeper water masses (~1500–3800 m) belong to the Indian Deep Water, which stems from the Lower Circumpolar Water through the Mascarene Basin between Seychelles and Madagascar (Johnson et al., 1991a, 1991b). Currents within the Indian Deep Water flow southwards in the Owen Basin (Fig. 2c; Reid, 2003).

3. Dataset and methods

Partial multibeam bathymetry coverage of the Sawqirah Ridge, 3.5 kHz mud penetrator and 24-channel seismic data were collected during the OWEN-2 (2012) cruise on board the BHO Beautemps-Beaupré. The SBP120 sub-bottom profiler was coupled with the Kongsberg-Simrad EM 120 multibeam echosounder, and provided a set of high frequency (3.5 kHz), high-resolution profiles with penetration down to 100 m in fine grained sediments. Seismic reflection profiles were acquired at ~10 knots using two GI air-guns (one 105/105 c.i. and one 45/45 c.i. fired every 10 s at 160 bars in harmonic mode, resulting in frequencies ranging from 15 to 120 Hz) and a 24-channel, 600 m-long streamer, implying a common mid-point spacing of 6.25 m. A sub-surface penetration of about 2 s two-way travel time (TWT) was achieved throughout the survey. The processing consisted of geometry setting, water-velocity normal move-out, stacking, water-velocity F-k domain post-stack time migration, bandpass filtering and automatic gain control.

The OWEN dataset is completed with seismic lines previously collected during the pre-site survey for ODP Leg 117 (Shipboard Scientific Party, 1989). The entire seismic dataset is tied with ODP drillings available in the Arabian Sea (Shipboard Scientific Party, 1989) to provide the stratigraphic framework. Conversion from two way travel time (in s TWT) to water depth (in m) was performed using a P wave velocity of $1550 \text{ m} \cdot \text{s}^{-1}$ measured at ODP Site 728 for the uppermost sediments (~100 m below the seafloor).

4. Results

4.1. The Sawqirah anticline system

The Sawqirah Anticline System (Figs. 4, 5) deformed Early to Late Miocene turbidites and inter-bedded Mass Transport Deposits (MTD hereafter; Shipboard Scientific Party, 1989; Rodríguez et al., 2014a). A series of antiforms and synforms compose the anticline system, with wavelengths ranging from 12 to 25 km and amplitude varying from 0.1 to 1-km on transverse (Figs. 4, 5) and longitudinal (Figs. 6–8) profiles. A dense network of unevenly distributed faults irregularly offsets the anticline system (maximum offset in the order of 0.1 s TWT, Figs.

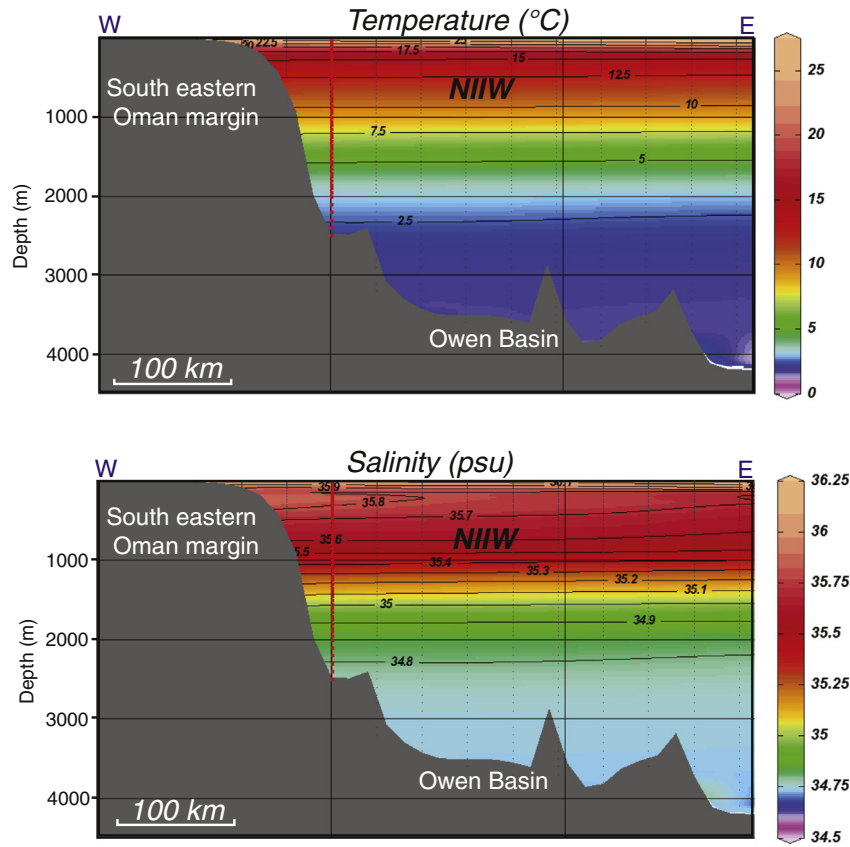


Fig. 3. Temperature and salinity E-W profiles of water masses in the Owen Basin, crossing the South East Oman margin. NIW: North Intermediate Indian Water.

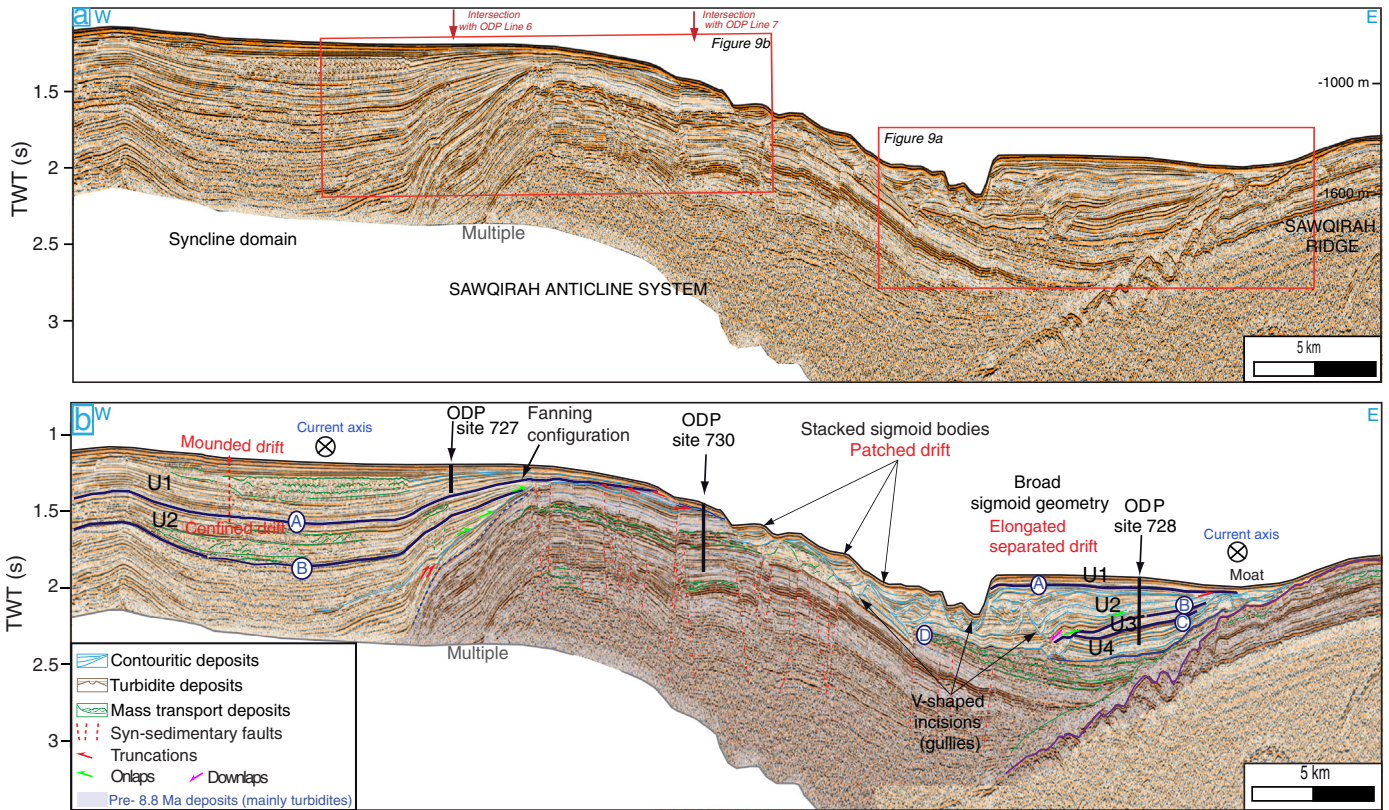


Fig. 4. a) Seismic profile (OWEN cruise) crossing the Sawqirah Bay and the Sawqirah Ridge at the South East Oman margin, and b) its interpretation. Units U1 to U4 and unconformities A to C: see text. The profile shows a major anticline structure affecting chalk-rich turbiditic deposits, overlapped by a post-8 Ma contourite drift. To the west, a confined drift evolving in a mounded drift is observed, whereas a separated drift is observed to the east. See Fig. 2 for location.

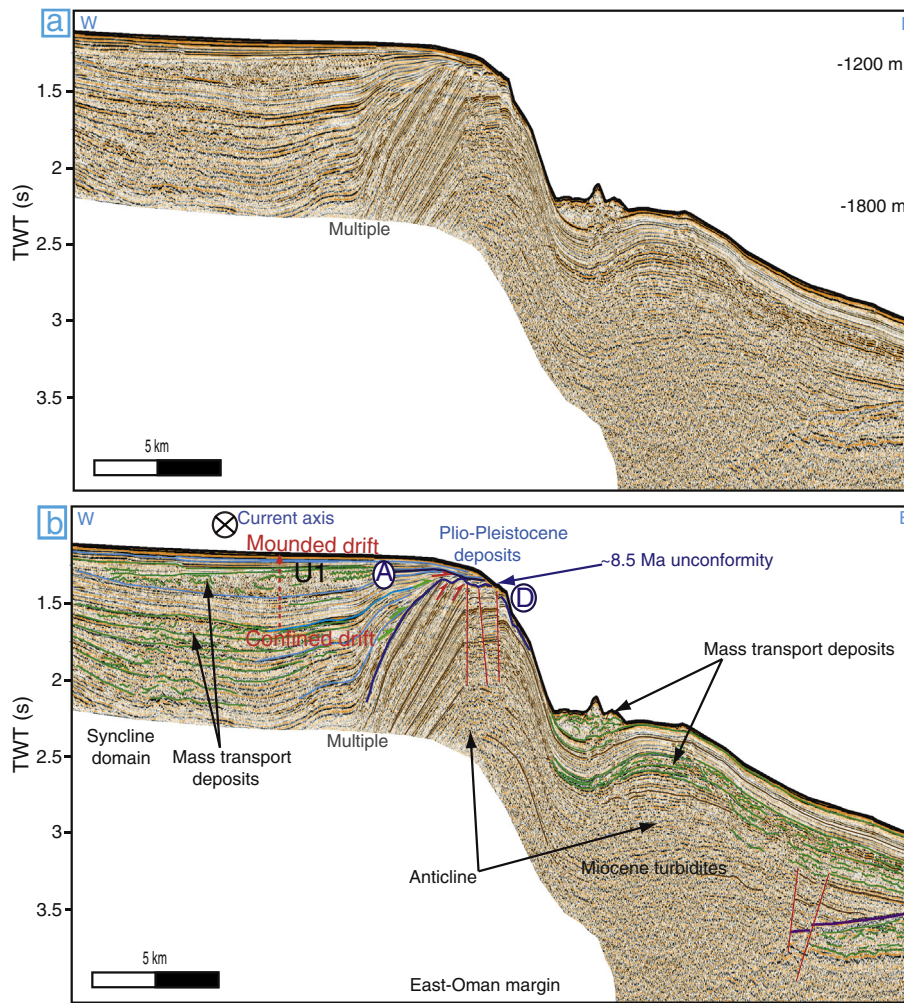


Fig. 5. Seismic line (OWEN cruise) crossing the Sawqirah Anticline and the confined area of the Sawqirah Drift. Unit U1 and unconformity A: see text See Fig. 2 for location.

4–8). This fault pattern can be either related to the folding or to fluid circulation, but also to differential compaction within the sediments (Rodriguez et al., 2014a, 2016).

4.2. Seismic stratigraphy of post-Late Miocene deposits

The Sawqirah Anticline System controls the distribution of the post-Late Miocene sediments derived from the Oman margin, most of them being trapped on the western side of the anticlinorium on transverse sections (Figs. 2, 4, 5). The post-Late Miocene sediments are composed of silty clays, calcareous ooze and chalk, in variable proportions (Fig. 9, Shipboard Scientific Party, 1989). Several angular unconformities recognized within the post-Late Miocene strata define stratigraphic units corresponding to distinct episodes of sedimentation (Figs. 4–9). Landslides scars and MTDs are commonly observed, on both seismic and multibeam data (Figs. 2; 4–8).

ODP Site 728 provides stratigraphic constraints down to the Late Miocene on the eastern side of the Sawqirah Anticline System (Fig. 9a), but these ages cannot be correlated over the entire anticline system. On the western side, the deepest ODP Site 726 only reaches 3.5 Myrs-old sediments (Fig. 9 b, c). All other sites have a limited penetration, and only document sediments younger than 1.9 Ma. In the absence of deep-penetrating drillings, the complex pattern of the Sawqirah Anticline System precludes reliable stratigraphic correlations based on seismic profiles from one flank of the anticline to another.

4.2.1. Unconformity A

The most recent seismic unconformity is labeled A on seismic and echosounder data (Figs. 4–10). Toplap truncations of the underlying strata, well expressed in the vicinity of anticline highs, indicate that the surface is locally an erosional unconformity (Figs. 4, 9, 10). The A-unconformity is outlined by erosive truncations in the vicinity of a slope-sourced canyon (northern section of ODP Line 6, Fig. 7). In some places, the erosional unconformity becomes conformable with the underlying sedimentary layers (as at ODP Site 724 (Fig. 4c), or in some segments of ODP Line 6, Fig. 7). The A-unconformity can be correlated over the entire study area and is therefore of regional extent. The best stratigraphic control is provided at ODP Site 728, in the eastern part of the anticline (Figs. 4, 6). There, the unconformity is located 67.5 m below the seafloor (mbsf) and is dated at 2.4 Ma by the first appearance in the sedimentary record of the calcareous nannoplankton *Discoaster surculus*. In the western part of the anticline, limited penetration at ODP Sites 723 and 727 only allows the identification of a 1.9 Myr-old reflector (Figs. 4, 6). The A-unconformity is observed 0.1–0.2 s (TWT) below this 1.9 Myr-old reflector (Figs. 4, 6) and can be correlated from line to line throughout the Sawqirah Bay area, where it is dated at 2.4 Ma at ODP Site 724 (North Eastern part of the Sawqirah Bay, Fig. 9c), consistently with estimates at ODP Site 728. The hiatus related to the unconformity A is highly variable throughout the Sawqirah area. Where the erosive surface cuts into the Sawqirah Anticline System, the hiatus can be as high as ~7.5 Myrs (at ODP Site 730, Figs. 2, 4; Shipboard Scientific Party, 1989). Where the erosive surface cuts into

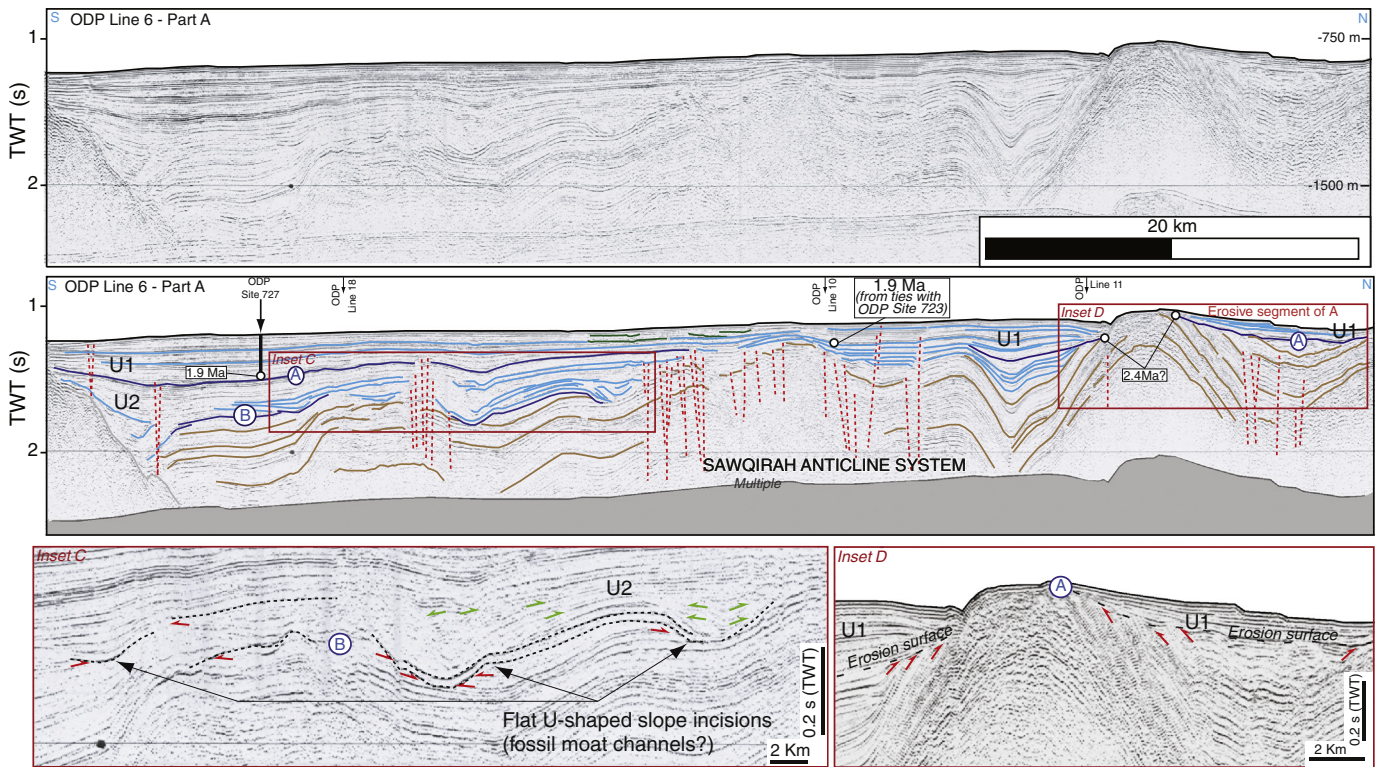


Fig. 6. a) Uninterpreted and b) Interpreted southern part of ODP seismic line 6 showing the longitudinal structure of the Sawqirah Anticline system and the architecture of the Sawqirah Drift. Ties with ODP Sites 723 and 727 locally constrain the stratigraphy. c) Inset highlights the U-shaped incisions at the base of Unit 2. d) Inset highlights the erosive pattern of the unconformity A, underlined by toplap truncatures. Units U1 and U2 and unconformities A and B: see text See Fig. 2 for location.

the post-Late Miocene sedimentary cover, the hiatus can be on the order of ~1 Ma (at ODP Site 726, Fig. 2; Shipboard Scientific Party, 1989).

4.2.2. Stratigraphic Unit 1 (between unconformity A and the seafloor)

Unit 1 is associated with lateral thickness variation and an overall sigmoid geometry due to strata pinching out against the anticline highs, on both longitudinal (N-S) and transverse (W-E) sections (Figs. 4–8). Numerous MTD are observed within Unit 1, especially in the south-western part of the anticline system (Fig. 4). Along the continental slope, Unit 1 is locally affected by erosional submarine canyons (ODP Line 6, Fig. 7). There, Unit 1 displays a sigmoid architecture, with progradation of the reflectors towards the canyon axis (Fig. 7). The edges of these canyons are locally associated with steep erosional scars interpreted as the result of mass-wasting processes (Figs. 7 and 8). Unit 1 also shows a conspicuous sediment wave pattern on the southern part of the anticline (ODP Line 7, Fig. 8), corresponding to an undulated seafloor or semi-circular depression fields on the multibeam bathymetry (Fig. 2), here interpreted as sediment waves. Sedimentation rates are highly variable since 1.9 Ma according to the location, and range from 60 to 130 $\text{m} \cdot \text{Myr}^{-1}$ at ODP Site 727, from 130 to 240 $\text{m} \cdot \text{Myr}^{-1}$ at ODP Site 723, from 11 and 34 $\text{m} \cdot \text{Myr}^{-1}$ at ODP Site 728 (Shipboard Scientific Party, 1989).

4.2.3. Unconformity B

A deeper unconformity is observed in various places of the Sawqirah Anticline System. The unconformity forms either flat, U-shaped incisions (inset Fig. 6c) or V-shaped incisions (southern flank of the anticline system, Fig. 8). In the eastern part of the Sawqirah Anticline System, at ODP Site 728, the unconformity is found at ~220 mbsf (Shipboard Scientific Party, 1989) and dated at 4.7–4.8 Ma (*Solenosphaera omnitubus*) (Figs. 4, 9). At ODP Site 728, the hiatus associated with unconformity B is of 0.3–0.5 Myrs (Shipboard Scientific Party, 1989). In the western part of the Sawqirah Anticline System, the

unconformity is recognized between 1.6 and 1.8 s (TWT) on the southern part of ODP line 6 (Fig. 6).

4.2.4. Stratigraphic Unit 2 (between unconformities B and A)

Conformable horizons characterize the uppermost part of the unit, except in the vicinity of anticline highs, where pinching-out of deposits occurs (Figs. 4, 6). In the eastern and southern parts of the anticline, Unit 2 is characterized by a broad aggradational sigmoid geometry. Slope incisions within Unit 2 display “V-shaped” erosional patterns outlined by truncated reflections (Figs. 6, 8). These incisions were gradually filled-in by sigmoid-shaped depositional bodies. Sedimentation rates between unconformities B and A are on the order of 88 $\text{m} \cdot \text{Myr}^{-1}$, but were reduced to 23 $\text{m} \cdot \text{Myr}^{-1}$ at the end of the unit deposition (at ODP Site 728, Shipboard Scientific Party, 1989).

Finally, two additional unconformities are only observed on the eastern part of the Sawqirah Anticline System, defining two local stratigraphic units.

4.2.5. Unconformity C

The unconformity C (Figs. 4, 9a) is 300 mbsf at ODP Site 728, and marked by downlap terminations of the overlying reflectors. The unconformity C is roughly dated around 6.1–6.7 Ma by the occurrence of *Stichocorys delmontensis* and *Stichocorys pereorina* (Shipboard Scientific Party, 1989), but biostratigraphic constraints are too scarce (low sampling resolution) to quantify any stratigraphic gap.

4.2.6. Stratigraphic Unit 3 (between unconformities C and B)

The Unit displays downlap terminations over unconformity C and lateral thickness variations (Figs. 4, 9). Sedimentation rates were on the order of 28 $\text{m} \cdot \text{Myr}^{-1}$.

4.2.7. Unconformity D

The oldest seismic unconformity, labeled D, is recognized at ~2.4–2.5 s (TWT) at ODP Site 728 (Figs. 4, 9) and is overlaid by a MTD. The

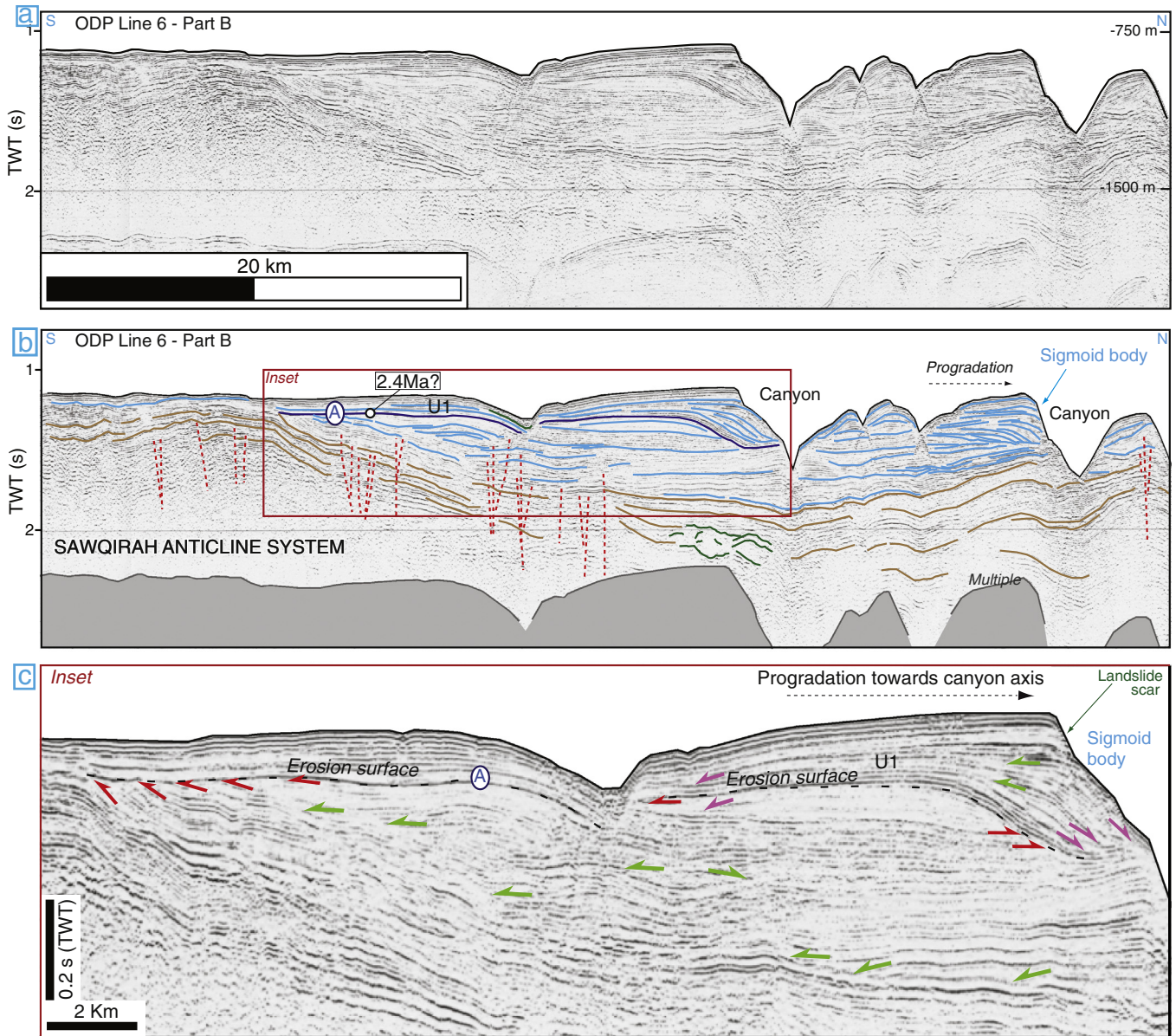


Fig. 7. a) Uninterpreted and b) Interpreted northern part of ODP Line 6, showing the longitudinal structure of the Sawqirah Anticline system and the architecture of the Sawqirah Drift. C) Inset shows a canyon related drift, and highlights the progradation of the drift towards the canyon axis. The erosive pattern of unconformity A is also underlined by toplap truncatures. See Fig. 2 for location.

age of the unconformity D is bracketed between 8.2 Ma (oldest sediments drilled at ODP Site 728) and 8.8 Ma (age of the youngest folded sediments at ODP Site 730).

4.2.8. Stratigraphic Unit 4 (between unconformities D and C)

A large MTD is identified at the base of the Unit 4 (Figs. 4, 9). It is overlaid by conformable and parallel horizons shaping the underlying morphology. Sedimentation rates are on the order of $28 \text{ m} \cdot \text{Myr}^{-1}$ (Shipboard Scientific Party, 1989).

4.3. Interpretation: The Sawqirah contourite drift system

Here we describe several types of drifts (classified according to Faugères et al., 1999; Rebesco et al., 2014) of different ages, defining the 'Sawqirah Contourite Drift system'. We expose the criteria for identification of the different types of drifts, i.e. the signature of bottom currents over the architecture of sedimentary deposits. A common particularity of most of the drifts described hereafter is the fact that they do not form downlap termination at their base, but onlap instead.

This is due to the steep slopes and the uneven topography of the Sawqirah Anticline System. The various types of drifts observed within the Sawqirah Drift System are summarized in Fig. 11.

4.3.1. Elongated separated drift

On the eastern part of the Sawqirah Anticline System, large thickness variations of sedimentary layers are observed, with pinching of sedimentary layers in the vicinity of the anticline highs (Fig. 4). It reflects lateral variation in current intensity, the weaker the current the thicker the sedimentary layers. The build-up of the drift at anticline flanks is characterized by the upslope migration of onlap terminations (Figs. 4, 5), which indicates the predominance of current influence over gravity-driven, mass wasting processes (Faugères et al., 1999). Along the eastern side of the anticline, the moat channel shown on the 3.5 kHz profile is built on the abrupt slope of the Sawqirah marginal ridge to the east, whereas the levee shows aggradation and migration of deposits in direction of the moat (Figs. 4, 10). This pattern of aggradation of sediments non-parallel to the accumulation surface (i.e. the

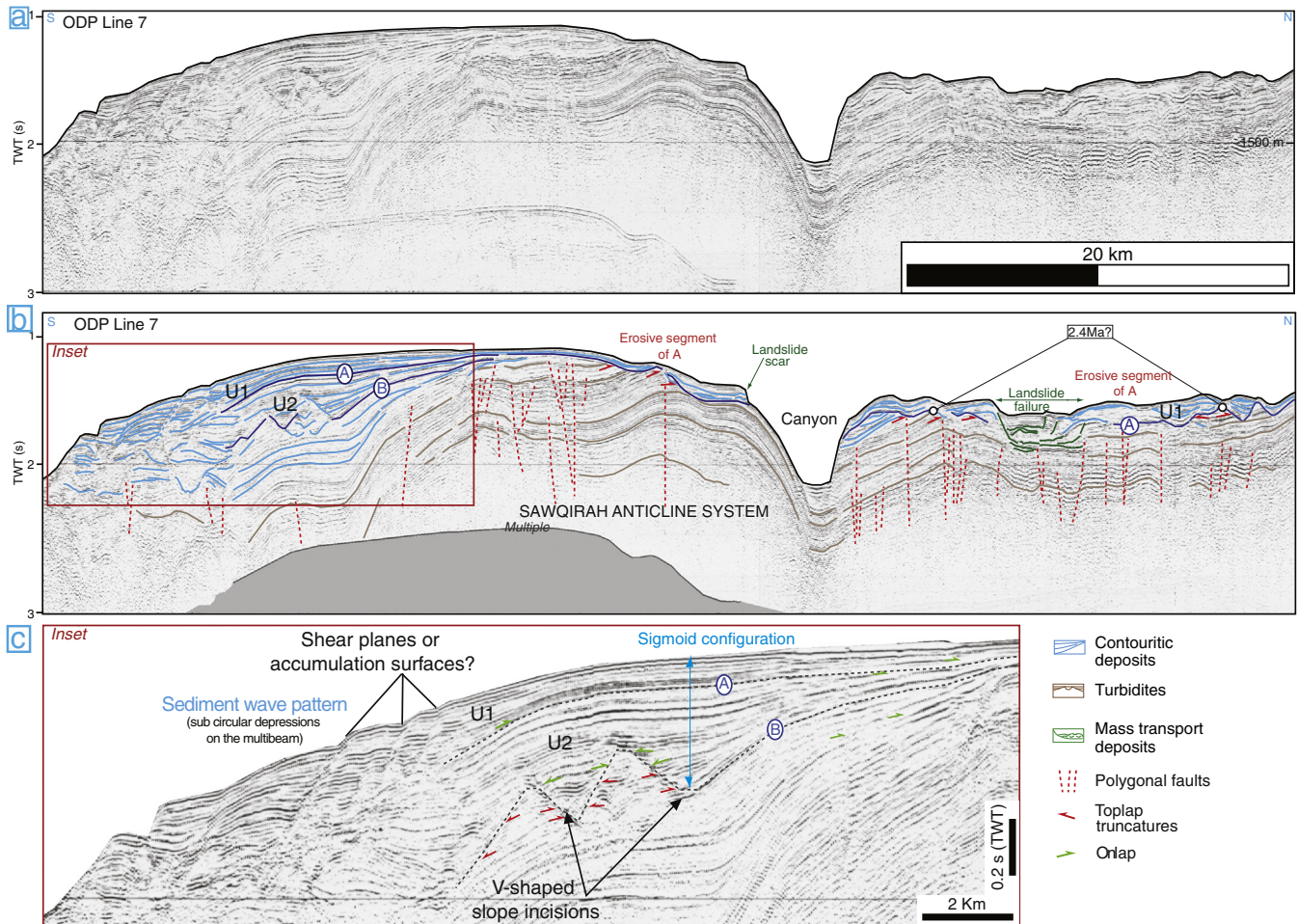


Fig. 8. a) Uninterpreted and b) Interpreted ODP seismic line 7 showing the longitudinal structure of the southern side of the Sawqirah Anticline system and the architecture of the Sawqirah Drift. Inset c) A conspicuous undulating to sigmoid body, and V-shaped slope incisions characterize the drift architecture on this seismic profile. Units U1 and U2 and unconformities A and B: see text. See Fig. 2 for location.

unconformities at the base of the units) characterizes both units 1 and 2. The moat channel indicates the main axis of the current, where the intensity is maximal, whereas the sigmoid geometry indicates a lateral weakening of current intensity. In this area, the current does not form a contouritic levee (no downlap terminations). The moat reflects reduced deposition rather than intense erosion after 2.4 Ma. The reflector corresponding to unconformity A locally displays the characteristics of an erosive surface (underlain by erosive truncations, see Figs. 4, 6 inset d), but laterally becomes part of a package of conformable, aggradational reflectors. The erosive pattern is observed where the intensity of the current is strong, whereas the conformable, aggradational pattern is observed in areas where the current intensity is weaker, allowing deposition (Faugères et al., 1999). These features are typical of an elongated, separated drift, where the main bottom current sweeps the Sawqirah Ridge, and builds a sigmoid levee on its left hand side.

4.3.2. Confined and mounded drift

Within the syncline domains of the Sawqirah fold system (western part; Figs. 4, 5), the architecture of the sedimentary cover shows an upward decrease of the concavity of reflectors, reflecting the progressive infill of the syncline. Reflectors become convex once the sedimentary infill reaches the apex of the anticline. MTDs trapped in the syncline (Figs. 4, 5) helped to cover-up the fold system, and locally enhanced the thickness of the stratigraphic units. In the vicinity of anticline highs, pinching-out of sedimentary layers occurs, as well as upward migration of onlap terminations, indicating here again the control of bottom current over deposition. The main axis of the current was

confined in the syncline domain, with a lateral decrease of its intensity in the vicinity of the anticline highs. Anticline highs limited any lateral migration of the drift along the E-W direction. The anticline highs enclosed a confined drift, until there were fully covered by sediments. Then, the confined drift turned into a mounded drift (Figs. 4, 5).

4.3.3. Multi-processes generated sediment waves

Along the southern side of the Sawqirah Anticline System, a sigmoid body shows an internal sediment wave pattern above unconformity A on ODP line 7 (Fig. 8), and a field of subcircular depressions on the multibeam (Fig. 2). It is unclear whether some discontinuities in reflectors reflect shear planes or steep accumulation surfaces. The wavelength of the sediment waves increases downslope. The sediment wave pattern and the subcircular depressions field can result either from interactions with bottom current, or creeping within the sediments in response to locally steeper slopes, or the combination of both processes. This feature is classified as a multi-processes generated sediment waves (similar to configurations described elsewhere by Faugères et al., 2002; Shillington et al., 2012).

4.3.4. Canyon related drift and contourite infill of slope incisions

Slope incisions (V- or U-shaped incisions) introduce local interactions with bottom currents, and induce second-order complexities in the seismic architecture of the Sawqirah Drift. V-shaped incisions observed within Unit 2 on the southern and eastern sides of the Sawqirah Anticline System (Figs. 4, 8) are interpreted as fossil gullies formed by downslope flowing gravity currents. The buried, flat U-shaped incisions

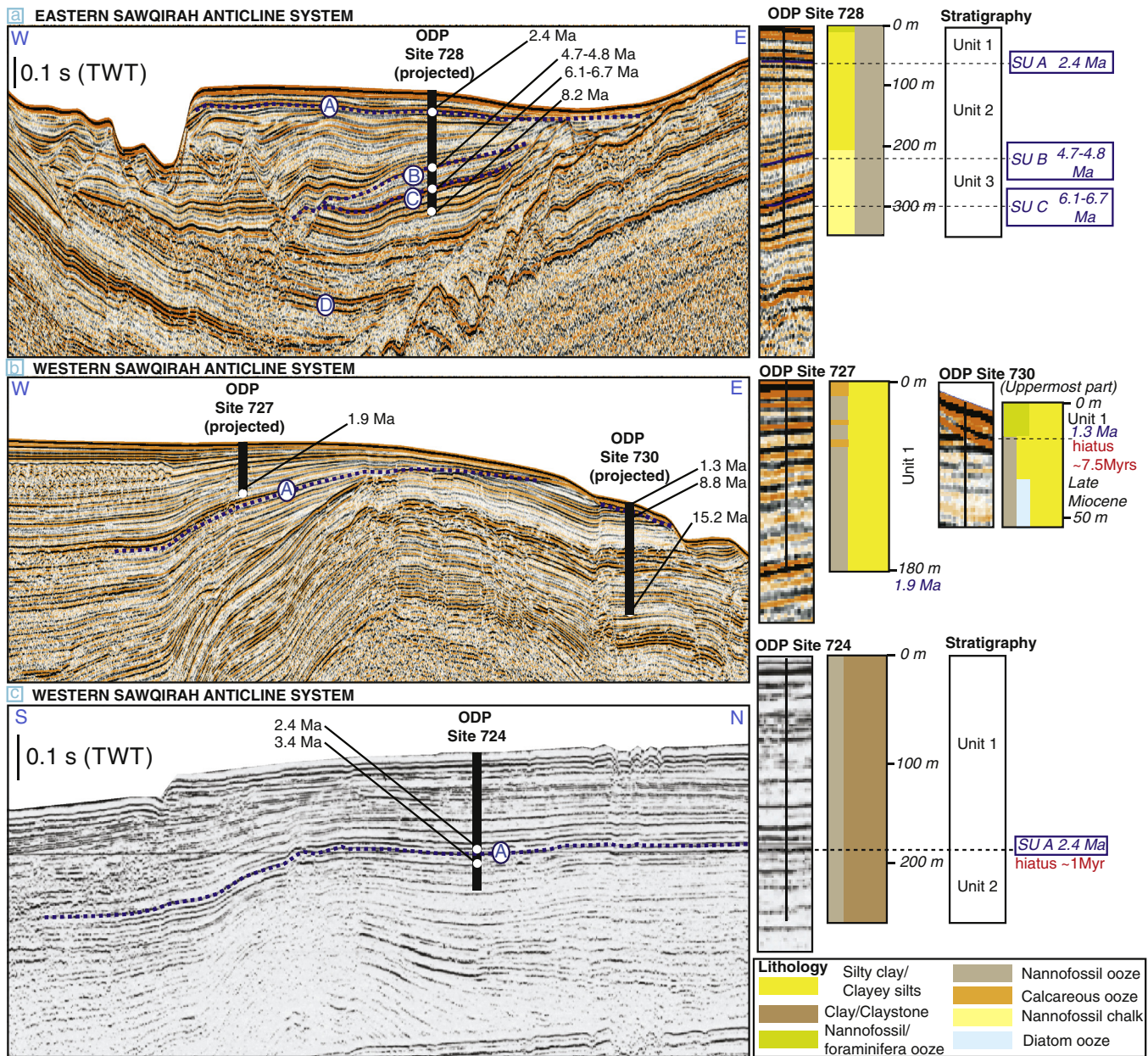


Fig. 9. Calibration of seismic profiles with ODP drilling sites, and lithology of the drilling sites; a) calibration of the ODP Site 728 in the Eastern Sawqirah Anticline System; b) and c) calibration of ODP Sites 727 and 730 in the Western Sawqirah Anticline System. Four unconformities, labeled from A to D, are observed. Units 1 to 3: see text.

identified at the base of Unit 2 on the western side of the Sawqirah Anticline System (Fig. 6) show a configuration close to the moat channel identified on the 3.5 kHz profile (Fig. 10) within Unit 1 on the eastern side of the Sawqirah Anticline System, which strongly suggests the incisions where the axis of paleocurrents.

Various drift geometries are observed in association with slope incisions. In the northern part of ODP Line 6 (Fig. 7), within Unit 1, progradation of the sedimentary layers towards the axis of the gully is observed. There, progradation and sediment deposition preferentially occur on the southern flank of the gully, which highlights the difference in current strength from one flank of the gully to the other. The gully captures the current, which erodes preferentially the northern flank of the gully, and promotes deposition on the opposite flank, forming the sigmoid configuration (Fig. 7). The same type of asymmetric sigmoid bodies commonly filled-in gullies in Unit 2 (Figs. 4, 9) in the eastern part of the drift. Small patched, sigmoid drifts are commonly observed

at the head of gullies (Figs. 2; 4, 8), and reflect local disturbances of the bottom current in the vicinity of the slope incision.

5. Discussion

5.1. Formation and evolution of the Sawqirah contourite drift system

The history of the Sawqirah Drift System involves complex interactions between the uplift of the Sawqirah Anticline System and variations of the intensity of the bottom current (summarized in Fig. 12). The reconstruction of the tectonic and sedimentary evolution of the Sawqirah area is limited due to the lack of quantification of uplift rates since the Late Miocene, the lack of stratigraphic constrains in some parts of the drift, and the lack of a denser seismic coverage of complex parts of the drift. Despite these limitations, the dataset allows us to propose a first-order reconstruction of the evolution of the system.

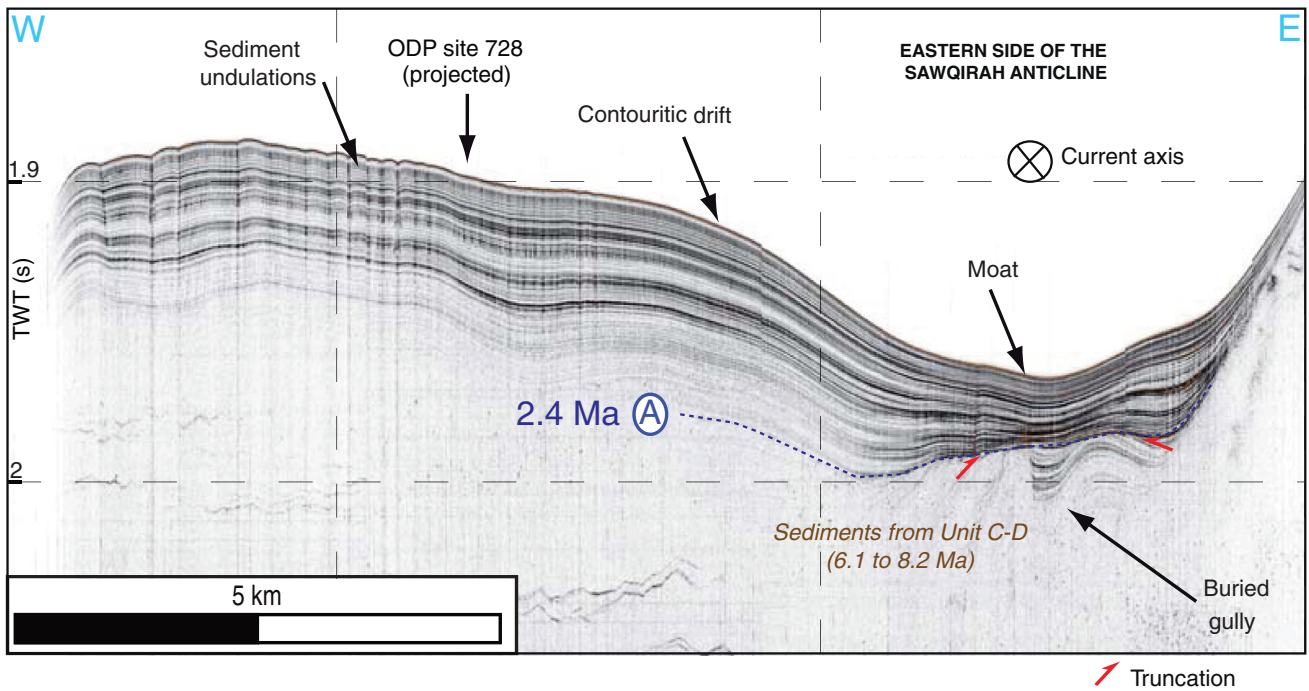


Fig. 10. High-resolution 3.5 kHz echo-sounder profile showing the uppermost part of the Sawqirah separated drift. A contouritic moat and the erosive pattern of the unconformity A are observed. See Fig. 2 for location.

The ~8.2–8.8 Ma-old D-unconformity corresponds to the onset of the tectonic deformation at the Sawqirah Anticline System (Fig. 12, Rodriguez et al., 2014a). Deformation triggered submarine landslides, with some MTDs now buried under the sedimentary cover (e.g. the MTD buried under the separated drift to the east on Fig. 4) and other landslides still expressed at the seafloor (Figs. 2, 5). The sedimentary sequence between C and D unconformities does not display any feature associated with contourite drifts.

The C-unconformity was dated at 6.1–6.7 Ma (Figs. 4, 9a), which may correspond to the onset of the influence of bottom currents on sedimentation along the eastern flank of the Sawqirah Anticline System (downlap terminations over unconformity C; Fig. 9a). This unconformity is hardly identified elsewhere in the drift, making it difficult to assess whether it corresponds to the onset of contourite build-up at the scale of the entire Sawqirah area, or just on a narrow part of the anticline system. The time gap between the beginning of the deformation around 8–9 Ma and the possible first record of contourite at 6.1–6.7 Ma may reflect the time needed to uplift the seafloor to a depth where currents were strong enough to influence the sedimentary architecture. It is however difficult to say if the contourite record reflects the activity of currents within the NIW or deeper currents at that time. Fig. 12 presents a configuration where contourite deposition began at 6.1–6.7 Ma in the entire Sawqirah area.

The B-unconformity (4.7–4.8 Ma in ODP site 728) marks a change in the intensity of the current. Locally, moat channels developed along anticline flanks (ODP Line 6; Fig. 6; ODP Line 7; Fig. 8), indicating intensification of bottom currents at the beginning of the sequence recorded by Unit 2. The deposition of Unit 2 was characterized by complex interactions between bottom current and slope incisions.

The A-unconformity (2.4 Ma) corresponds to an uneven peneplanation surface of the Sawqirah Anticline and Drift system, interpreted as a result of intensified contour current-driven erosion (Fig. 12). On the eastern side of the anticline, a new contouritic moat emplaced immediately above the A-unconformity, pointing out a shift in the axis of the main current, consistent with a reorganization of the oceanic circulation pattern at that time (Figs. 4, 10). Along the western flank of the Sawqirah Anticline System, the confined drift caught-up the

top of the anticline during the Pleistocene, and turned into a mounded drift (Figs. 4, 5). The A-unconformity has previously been interpreted as the result of the subaerial exposure of the anticline, but this is not supported by the evidence of unconformity A being formed and preserved away from the apex of the anticlinorium (Figs. 4–8). The uplift of the anticline is therefore ~1000 m less than what was previously proposed (Shipboard Scientific Party, 1989).

5.2. Building of the Sawqirah drift: Interactions between tectonic processes and oceanic currents

5.2.1. Interplay between the Sawqirah anticline system and the Coriolis force

The Coriolis force is a major control factor of the evolution of contourite drifts. However, in the case of the Sawqirah Contourite Drift System, the uneven topography of the substratum of the drift together with the local steep slopes, may promote the steering of currents and locally increase their velocity, so the flow becomes ageostrophic, and the influence of Coriolis force becomes negligible (especially at latitudes lower than 20°N; Cossu et al., 2014). It is therefore difficult to highlight the role of the Coriolis force over the development of the Sawqirah Drift System.

5.2.2. Interplay between the Sawqirah anticline system and the evolution of the Sawqirah contourite drift system

Although the development of the anticline has ceased, its morphology is still a first-order control on the extent of the drifts, their thicknesses, and the sedimentary expression of spatial variations of current intensity. For instance, the configuration of the confined drift trapped in the syncline (western side of the Sawqirah anticline) highlights that the current was more intense in the middle of the syncline than on its flanks, where contouritic levees built-up (Figs. 4, 5). The contouritic moats (U-shaped incisions) at the base of Unit 2 are localized only in the syncline parts, which may indicate the syncline trapped local eddies there. The fold system acted as a topographic barrier for the sediments coming from land, being trapped in the syncline domains, and localizing

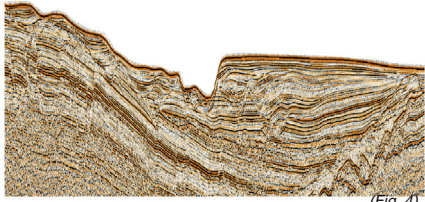
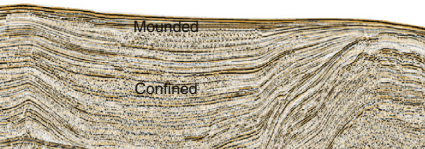
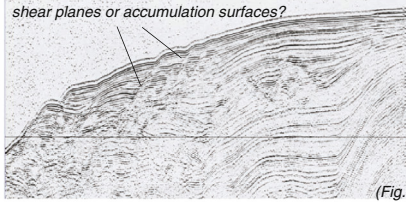
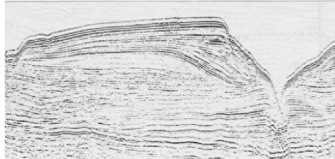
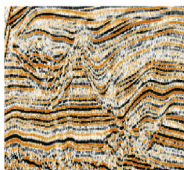
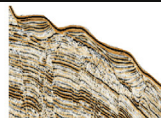
Contourite drift nomenclature	Description & Process	Examples of drift architecture from the Sawqirah Drift (Arabian Sea)	
Elongated Separated Drift	<ul style="list-style-type: none"> *Aggradation non-parallel to the accumulation surface *Sigmoid bodies, limited either by downlaps or truncatures *Discontinuities (Hiatuses) within the drift, reflecting variations in current intensity * Moat channels 	 (Fig. 4)	
Confined and mounded drift	<ul style="list-style-type: none"> * Drift confined between anticline highs *Fanning of sediments close to anticline flanks 	 (Fig. 4)	
Multi-processes generated sediment waves	<ul style="list-style-type: none"> * Wavy reflectors, forming asymmetric bodies * Whether these bodies lie on shear planes or steep accumulation surfaces is ambiguous *Interaction between current, creeping, slope instability processes? 	 (Fig. 8)	
Drift related to slope incisions	Canyon related drift	<ul style="list-style-type: none"> * Sigmoid architecture, with onlaps terminations outside of the canyon influence, and downlaps and truncatures close to the canyon * Migration and preservation of the slope incision during the building of the drift 	 (Fig. 7)
	Contourite infill of slope canyons/gullies	<ul style="list-style-type: none"> *Slope incisions revealed by truncated reflectors *Infill: sigmoid to asymmetric bodies. The current is channeled along a canyon's flank and erodes it. The eroded material is deposited on the other flank of the canyon, where the current is weaker. 	 (Fig. 4)
	Patched drift	<ul style="list-style-type: none"> *Small sigmoid bodies stacked within slope incisions in various places of the anticline flanks 	 (Fig. 4)

Fig. 11. Synthesis of the various types of contourite drift architectures observed off Oman.

the development of mounded drifts once the syncline has been fully infilled. The influence of MTDs over the architecture of the drift is major in syncline areas where they are trapped, and negligible along the open-slope flanks of the anticline where they are released to the Owen Basin. The steepness of the flanks of the anticline influences the distribution of creeping within the sedimentary cover (e.g. southern side of the anticline, Fig. 8).

However, the anticline does not control the pattern of the erosive unconformity A. At the time of formation of unconformity A (i.e. ~2.4 Ma), deformation was inactive (no tectonic deformation is recorded in the Owen Basin since at least the inception of the Owen Fracture Zone ~3 Ma, Fournier et al., 2011; Rodriguez et al., 2011; 2013; Rodriguez et al. 2014a, 2014b). Current intensification 2.4 Ma induced the widespread erosion of the underlying topography. Erosion locally flattened areas that used to be steep parts of the anticline (Figs. 6, 7, 8). Erosion due to bottom-currents can therefore reshape the anticline, and cancel its control over the development of the contourite.

5.3. The Sawqirah drift and the oceanic circulation in the Arabian Sea

Here we correlate the timing of drift sedimentation with the multi-proxies paleoclimatic and paleoceanographic records (Fig. 13) to investigate the possible significances of the two major unconformities (A and B) identified at Sawqirah. We keep in mind that the lack of studies of contourites in the Indian Ocean makes speculative the discussion of regional circulation changes from a single locality. Although discontinuities may occur within water masses and bottom currents (Lozier, 2010), we consider water mass continuity at the scale of 10^5 – 10^6 years.

5.3.1. Significance of the A-unconformity

The A-unconformity is synchronous with the onset of the Early Pleistocene Indian monsoon intensification at ~2.4 Ma defined by numerous paleoclimatic proxies (Fig. 13, Bloemendal et al., 1993; An et al., 2001; DeMenocal, 2004; Wan et al., 2012). This intensification of the monsoon is interpreted as the shift from strong precessional forcing (23 kyr) to a

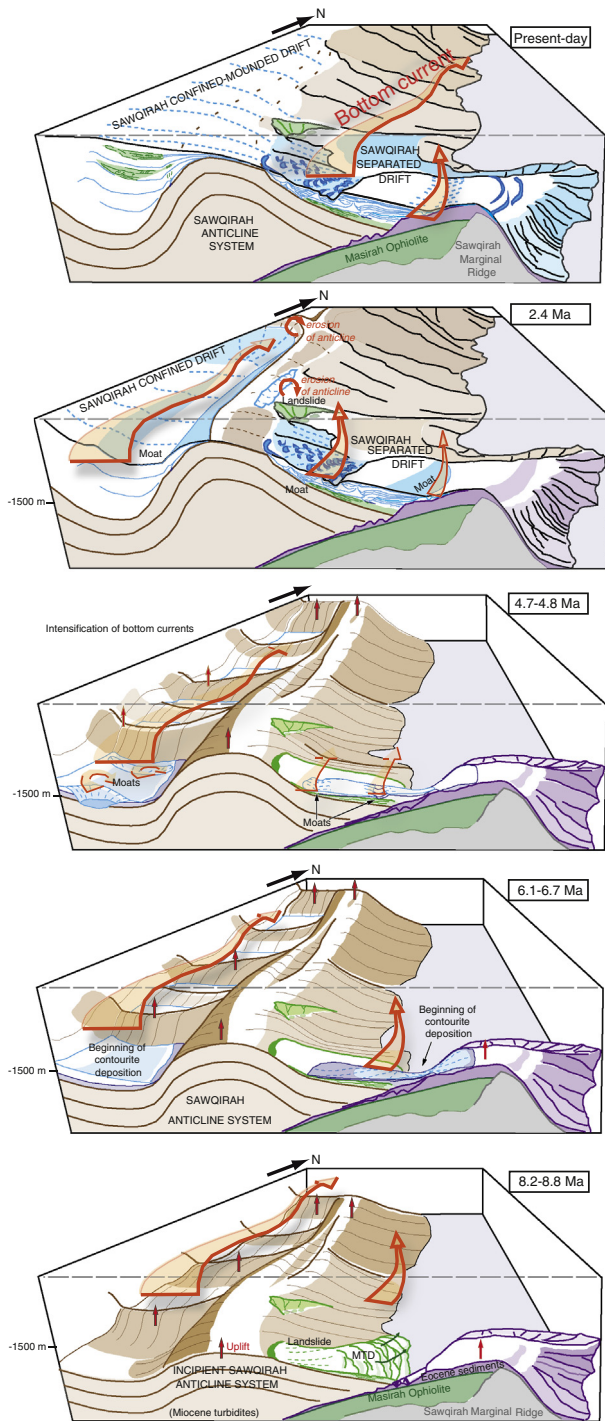


Fig. 12. Sketches of the formation of the Sawqirah Drift in interaction with the development of the Sawqirah Anticline system along the South East Oman margin. From bottom to top: -The 8.2–8.8 Ma stage (unconformity D) corresponds to the onset of folding, marked by the triggering of large submarine landslide. The seafloor is too deep to record the activity of bottom current within intermediate waters. -The 6.1–6.7 Ma stage (unconformity C) corresponds to the beginning of the building of the Sawqirah Drift, the seafloor being now high enough to catch the activity of the intermediate water bottom current. This unit is characterized by downlap terminations. This age of beginning of the drift is only constrained on the eastern side of the anticline system (ODP Site 728) but it is assumed here that it is roughly the same everywhere else in the Sawqirah Drift. -The 4.7–4.8 Ma stage (Unconformity B) marks the development of important slope incisions within the Sawqirah Drift, either related to slope processes (canyons, gullies) or bottom current (moats). This stage is interpreted as an intensification of the oceanic circulation, related to the coeval onset of upwelling in the Owen Basin. -The 2.4 Ma stage (Unconformity A) marks a regional intensification of the oceanic currents (locally eroding the anticline system), in response to the coeval intensification of the Asian Monsoon.

strong obliquity forcing (41 kyr) at the beginning of the Pleistocene (Bloemendal and DeMenocal, 1989; Clemens et al., 1996). The intensification of monsoon winds and the closure of the Indonesian Seaway 3–4 Ma helped the shoaling of the thermocline (Karas et al., 2009). The rise of the thermocline allowed the upwelling of the intermediate waters, which resulted in a net increase of planktonic productivity since 2.4 Ma recorded by abundances of *G. bulloides* in the pelagics of the Owen Ridge (Fig. 13, Huang et al., 2007). The bottom current shaping the Sawqirah Drift may have intensified in response to the enhanced coupling between atmospheric and oceanic circulation. Even if the thermocline is only ~200-m-deep, the intensity of currents within intermediate waters (200–1500 m) are affected by upwelling processes, as shown for West Africa (Séranne and Abeigne, 1999).

The A-unconformity is also synchronous with possible indicators of large-scale changes in the oceanic circulation of the Indian Ocean. According to ODP drilling sites on the South-East Oman margin (Shipboard Scientific Party, 1989), the NIW captured waters coming from the Red Sea, the Persian Gulf and the Gulf of Aden around the Late Pliocene (Hermelin, 1992), although a precise dating is lacking. Moreover, geochemical studies based on Neodymium (Nd) isotopes analysis from various Indian Ocean sediment cores defined a main paleo-current in the Indian Ocean, referred as the Miocene Indian Ocean Equatorial Jet (MIOEJ, Fig. 1b, Gourlan et al., 2008). The MIOEJ extended from the sea surface to intermediate depths (~1500 m) at equatorial latitudes, linking the eastern and the western Indian Ocean from ~14 Ma to ~3 Ma (Fig. 1b; Gourlan et al., 2008). A drastic change in Nd seawater record occurred around 2.5–3 Ma (Gourlan et al., 2008), which could either reflect a change in the oceanic circulation pattern following the closure of the Indonesian Seaway (Fig. 13; Cane and Molnar, 2001), or the increased weathering of the continents following the intensification of the Asian monsoon and/or the growth of mountain glaciers (Gourlan et al., 2008). The closure of the Indonesian Seaway 3–4 Ma (Cane and Molnar, 2001) helped the shoaling of the thermocline in the tropical Indian Ocean (Karas et al., 2009), which further disposed the Arabian Sea to upwelling.

5.3.2. Significance of the B-unconformity

B-unconformity is roughly coeval with an episode of cooling of Sea Surface Temperature in the Arabian Sea recorded at ~4.5 Ma, associated with a peak of *G. bulloides* abundances in marine sediments (Fig. 13, Huang et al., 2007). This episode reflects a transient intensification of upwelling of intermediate waters in the Arabian Sea (Huang et al., 2007). Intensification of upwelling may have induced strengthening of bottom currents at intermediate depths, forming the erosive features of unconformity B at Sawqirah. The thermocline needs to be shallow enough (200–300 m deep) for the winds to bring deep or intermediate cold water to the surface (Philander and Fedorov, 2003; Molnar et al., 2010). The thermocline of the world's oceans has gradually risen during the Cenozoic global cooling, and most of the present-day upwelling zones were emplaced only in the Late Pliocene–Early Pleistocene (Philander and Fedorov, 2003). The B-unconformity may thus record the time at which the thermocline was shallow enough to allow the development of upwelling along the Oman margin. The end of the ~4.5 Ma episode of upwelling may correspond to a period where the monsoon winds became too weak to sustain upwelling, in the context of the progressive weakening of the Indian monsoon (Clift et al., 2008; Steinke et al., 2010).

An alternative is to consider a transient episode of monsoon strengthening is at the origin of the episode of upwelling. The episode of monsoon strengthening is recorded by the dominance of C_4 plants and the lowering of $\delta^{18}O$ (–9‰) in the Siwalik paleosoil sequence in the Himalayan foreland (Sanyal et al., 2010). The end of the ~4.5 Ma episode of upwelling may have induced a weakening of bottom current circulation at intermediate depths, resulting in

Indian Monsoon evolution, and sedimentary events in the Arabian Sea

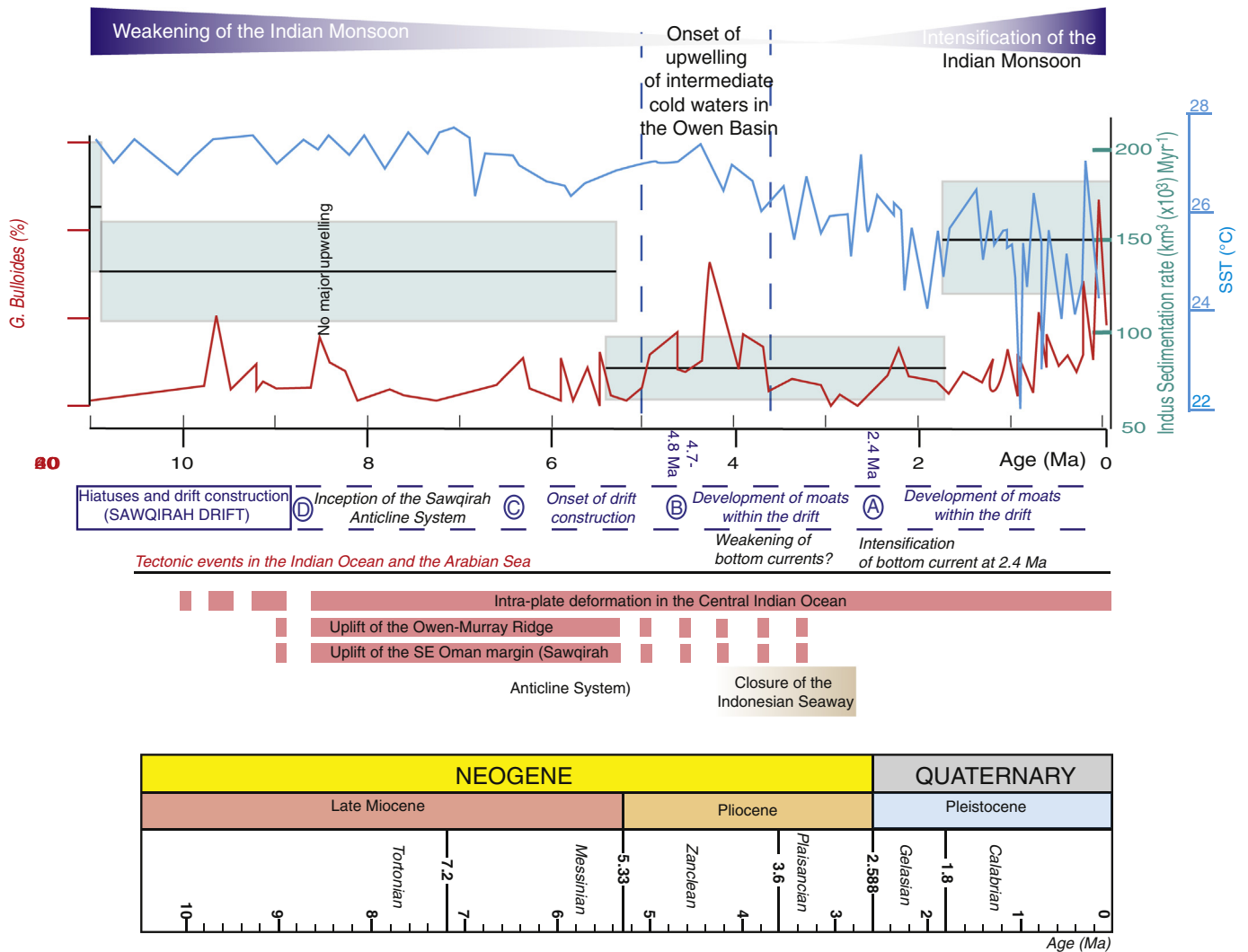


Fig. 13. Synthesis of climatic, sedimentary and paleoceanographic events in the Arabian Sea. Indus sedimentation rates are from Clift et al. (2008); *G. bulloides* abundances and SST (Sea Surface Temperature) variations are from Huang et al. (2007).

increasing sedimentation rates during the deposition of Unit 2 within the Sawqirah Drift.

However, marine records do not document the expected increase in sedimentation rates of the Indus turbiditic system that would result from a monsoon intensification around 4.5 Ma (Fig. 13, Clift, 2002; Clift and Blusztajn, 2005; Clift et al., 2008), neither do proxies of the Bengal system (Steinke et al., 2010). Therefore, the link between the 4.5 Ma episode of upwelling and monsoon intensification cannot be firmly established.

At the global scale, the episode of enhanced upwelling around 4.5 Ma occurred more than 1.3 Myrs earlier than in the Pacific and Atlantic oceans, where the onset of cold water upwelling is recorded at ~3.2 Ma (Marlow et al., 2000; Dekens et al., 2007). Several studies propose a shoaling of the thermocline and changes in depth of water masses starting around 4 Ma in the Pacific and Atlantic Oceans (see synthesis in Philander and Fedorov, 2003; Dekens et al., 2007; Filippelli and Flores, 2009; Molnar, 2008). The shoaling of the thermocline was possibly more efficient in the Arabian Sea due to the monsoon winds.

6. Conclusions

The Late Miocene uplift of a large Sawqirah Anticline System off the Oman margin favored the buildup of a contourite drift system recording the activity of bottom currents within the North Intermediate Indian Water. Contourite sedimentation probably initiated on the Sawqirah Anticline System after the Late Miocene (6.1–6.7 Ma), and more certainly from 4.7–4.8 Ma onwards. This age marks the time at which the anticline was developed enough to record the circulation of currents within the North Intermediate Indian Water. A wide range of contourite drift geometries are identified within the Sawqirah Contourite Drift System, including separated, confined, patched drifts and sediment waves. Major seismic unconformities within the Sawqirah Drift are interpreted as the result of major changes in bottom current activity during the late Cenozoic, which can be linked with the known climatic and oceanic changes around the Arabian Sea. For instance, the B-unconformity marks enhanced erosion and may be coeval with a temporary episode of upwelling of intermediate, cold waters off Oman at 4.5–5.5 Ma. The

origin of this oceanographic change remains difficult to determine since marine and terrestrial paleoclimate proxies contradict. The unconformity recorded another episode of intensification of oceanic circulation at 2.4 Ma, also highlighted by a surface of erosion. This paleocurrent intensification is thought to be the response to the coeval, well-defined episode of monsoon intensification following the onset of the Northern Hemisphere Glaciation.

Acknowledgements

We thank the cruise members of the R/V *Beautemps-Beaupré* as well as the GENAVIR team for their help in data acquisition during the cruises OWEN 1 & 2. Processing of the OWEN 2 seismic dataset was carried out using the GEOCLUSTER 5000 software of CGGVeritas. We sincerely acknowledge the very constructive comments provided by the Editor Michele Rebesco, Christian Betzler, and three anonymous reviewers, which helped us to significantly improve this paper. We are also grateful to Sabrina Speich for scientific discussions about oceanic circulation in the Indian Ocean. This study was supported by SHOM, IFREMER, and INSU-CNRS.

References

- Al Saafani, M.A., Shenoi, S.S.C., 2007. Water masses in the Gulf of Aden. *J. Oceanogr.* 63, 1–14.
- Allen, M.B., Armstrong, H.A., 2008. Arabia-Eurasia collision and the forcing of mid-Cenozoic global cooling. *Palaeogeogr. Palaeoclimatol. Palaeoecol.* 265, 52–58.
- An, Z., Kutzbach, J.E., Prell, W.L., Porter, S.C., 2001. Evolution of Asian monsoons and phased uplift of the Himalaya–Tibetan plateau since late Miocene times. *Nature* 411, 62–66.
- Bailey, I., Hole, G.M., Foster, G.L., Wilson, P.A., Storey, C.D., Trueman, C.N., Raymo, M.E., 2013. An alternative suggestion for the Pliocene onset of major northern hemisphere glaciations based on the geochemical provenance of North Atlantic Ocean ice-rafted debris. *Quat. Sci. Rev.* 75, 181–194. <http://dx.doi.org/10.1016/j.quascirev.2013.06.004>.
- Barton, P.J., Owen, T.R.E., White, R.S., 1990. The deep structure of the east Oman continental margin: preliminary result and interpretation. *Tectonophysics* 173, 319–331.
- Beal, L., Field, A., Gordon, A.L., 2000. Spreading of Red Sea overflow waters in the Indian Ocean. *J. Geophys. Res.* 105, 8549–8564.
- Ben-Avraham, Z., Niemi, T.M., Hartnady, C.J.H., 1994. Mid-tertiary changes in deep ocean circulation patterns in the Natal Valley and Transkei Basin, southwest Indian Ocean. *Earth Planet. Sci. Lett.* 121, 639–646.
- Betzler, C., Fürstenau, J., Lüdmann, T., Hübscher, C., Lindhorst, S., Paul, A., Reijmer, J.G., Droxler, A., 2013. Sea-level and ocean-current control on carbonate platform growth, Maldives, Indian ocean. *Basin Res.* 25, 172–196. <http://dx.doi.org/10.1111/j.1365-2117.2012.00554.x>.
- Bickert, T., Haug, G.H., Tiedemann, R., 2004. Late Neogene benthic stable isotope record of ocean drilling program site 999: implications for Caribbean paleoceanography, organic carbon burial, and the Messinian salinity crisis. *Paleoceanography* 19, PA1023. <http://dx.doi.org/10.1029/2002PA000799>.
- Billups, K., 2002. Late Miocene through early Pliocene deep water circulation and climate change viewed from the sub-Antarctic South Atlantic. *Palaeogeogr. Palaeoclimatol. Palaeoecol.* 185, 287–307. [http://dx.doi.org/10.1016/S0031-0182\(02\)00340-1](http://dx.doi.org/10.1016/S0031-0182(02)00340-1).
- Bloemendal, J., King, J.W., Hunt, A., DeMenocal, P.B., Hayashida, A., 1993. Origin of the sedimentary magnetic record at ocean drilling program sites on the Owen Ridge, Western Arabian Sea. *J. Geophys. Res.* 98, 4199–4219.
- Bloemendal, J., DeMenocal, P.B., 1989. Evidence for a change in the periodicity of tropical climate cycles at 2.4 Myr from whole-core magnetic susceptibility measurements. *Nature* 342, 897–900.
- Böhm, E., Morrison, J.M., Manghni, V., Kim, H.-S., Flagget, C.N., 1999. The Ras al Hadd jet: remotely sensed and acoustic Doppler current profiler observations in 1994–1995. *Deep-Sea Res.* II 46, 1531–1549.
- Bourget, J., 2009. Les systèmes Turbiditiques Du Golfe d’Oman et de La Marge Est-Africaine: Architecture, évolution Des Apports Au Quaternaire Terminal, et Impact de La Distribution sédimentaire Sur Les propriétés géoacoustiques Des Fonds (PhD thesis, 404 pp.) Univ. Bordeaux 1, France.
- Bourget, J., Zaragosi, S., Mulder, T., Schneider, J.-L., Garland, T., Van Toer, A., Mas, V., Ellouzi-Zimmermann, N., 2010. Hyperpycnal-fed turbidite lobe architecture and recent sedimentary processes: a case study. *Sediment. Geol.* 229, 144–159. <http://dx.doi.org/10.1016/j.sedgeo.2009.03.009>.
- Brink, K., Arnone, R., Coble, P., Flagg, C., Jones, B., Kindle, J., Lee, C., Phinney, D., Wood, M., Yentsch, C., Young, D., 1998. Monsoons boost biological productivity in the Arabian Sea. *EOS Trans. Am. Geophys. Union* 79, 168–169.
- Butzin, M., Lohmann, G., Bickert, T., 2011. Miocene ocean circulation inferred from marine carbon cycle modeling combined with benthic isotope records. *Paleoceanography* 26, PA1203. <http://dx.doi.org/10.1029/2009PA001901>.
- Cane, M.A., Molnar, P., 2001. Closing of the Indonesian seaway as a precursor to east African aridification around 3–4 million years ago. *Nature* 411, 157–162.
- Clemens, S.C., Murray, D.W., Prell, W.L., 1996. Nonstationary phase of the Plio-Pleistocene Asian monsoon. *Science* 274, 943–948. <http://dx.doi.org/10.1126/science.274.5289.943>.
- Clift, P.D., 2002. A brief history of the Indus River. *Geol. Soc. Lond., Spec. Publ.* 195, 237–258. <http://dx.doi.org/10.1144/GSL.SP.2002.195.01.13>.
- Clift, P.D., Blusztajn, J., 2005. Reorganization of the western Himalayan river system after five million years ago. *Nature* 438, 1001–1003. <http://dx.doi.org/10.1038/nature04379>.
- Clift, P.D., Hodges, K.V., Heslop, D., Hannigan, R., Van Long, H., Calvès, G., 2008. Correlation of Himalayan exhumation rates and Asian monsoon intensity. *Nat. Geosci.* 1, 875–880. <http://dx.doi.org/10.1038/ngeo351>.
- Clift, P.D., Wan, S., Blusztajn, J., 2014. Reconstructing chemical weathering, physical erosion and monsoon intensity since 25 Ma in the northern South China Sea: a review of competing proxies. *Earth-Sci. Rev.* 30, 86–102. <http://dx.doi.org/10.1016/j.earscirev.2014.01.002>.
- Cossu, R., Wells, M.G., Peakall, J., 2014. Latitudinal variations in submarine channel sedimentation patterns: the role of Coriolis forces. *J. Geol. Soc. Lond.* 172, 161–174. <http://dx.doi.org/10.1144/jgs2014.043>.
- Damuth, J., Johnson, D.A., 1989. Morphology, sediments and structure of the Amirante trench, western Indian Ocean: implications for trench origin. *Mar. Geol.* 6, 232–242.
- Dekens, P.S., Ravelo, A.C., McCarthy, M.D., 2007. Warm upwelling regions in the Pliocene warm period. *Paleoceanography* 22, PA3211. <http://dx.doi.org/10.1029/2006PA001394>.
- Delescluse, M., Montési, L.G.J., Chamot-Rooke, N., 2008. Fault reactivation and selective abandonment in the oceanic lithosphere. *Geophys. Res. Lett.* 35, L16312. <http://dx.doi.org/10.1029/2008GL035066>.
- deMenocal, P., 2004. African climate change and faunal evolution during the Pliocene-Pleistocene. *Earth Planet. Sci. Lett.* 220, 3–24.
- DeMets, C., Merkouriev, S., Sauter, D., 2015. High-resolution estimates of southwest Indian ridge plate motions, 20 Ma to present. *Geophys. J. Int.* 203, 1495–1527.
- Ercilla, G., Juan, C., Hernández-Molina, F.J., Bruno, M., Estrada, F., Alonso, B., Casas, D., Farran, M.L., Llave, E., García, M., Vázquez, J.T., d’Acremont, E., Gorini, C., Palomino, D., Valencia, J., El Moumni, B., Ammar, A., 2016. Significance of bottom currents in deep-sea morphodynamics: an example from the Alboran Sea. *Mar. Geol.* 378, 157–170.
- Faugères, J.C., Stow, D.A.V., Imbert, P., Viana, A., 1999. Seismic features diagnostic of contourite drifts. *Mar. Geol.* 162, 1–38.
- Faugères, J.C., Gonthier, E., Mulder, T., Kenyon, N., Cirac, P., Gribouard, R., Berné, S., Lesuavé, R., 2002. Multiprocess generated sediment waves on the Landes plateau (Bay of Biscay, North Atlantic). *Mar. Geol.* 182, 279–302.
- Filippelli, G.M., Flores, J.-A., 2009. From the warm Pliocene to the cold Pleistocene: a tale of two oceans. *Geology* 37, 959–960. <http://dx.doi.org/10.1130/focus102009.1>.
- Flagg, C.N., Kim, H.-S., 1998. Upper ocean currents in the northern Arabian Sea from ship-board ADCP measurements collected during the 1994–1996 U.S. JGOFS and ONR programs. *Deep-Sea Res.* II 45, 1917–1959.
- Fournier, M., Chamot-Rooke, N., Petit, C., Fabbri, O., Huchon, P., Maillot, B., Lepvrier, C., 2008. In-situ evidence for dextral active motion at the Arabia-India plate boundary. *Nat. Geosci.* 1, 54–58. <http://dx.doi.org/10.1038/ngeo2007.24>.
- Fournier, M., Chamot-Rooke, N., Rodriguez, M., Huchon, P., Petit, C., Beslier, M.-O., Zaragosi, S., 2011. Owen fracture zone: the Arabia-India plate boundary unveiled. *Earth Planet. Sci. Lett.* 302, 247–252. <http://dx.doi.org/10.1016/j.epsl.2010.12.027>.
- Gourlan, A.T., Meynadier, L., Allègre, C.J., 2008. Tectonically driven changes in the Indian Ocean circulation over the last 25 Ma: neodymium isotope evidence. *Earth Planet. Sci. Lett.* 267, 353–364.
- Gruetznert, J., Uenzelmann-Neben, G., 2016. Contourite drifts as indicators of Cenozoic bottom water intensity in the eastern Agulhas ridge area, South Atlantic. *Mar. Geol.* 378, 350–360. <http://dx.doi.org/10.1016/j.margeo.2015.12.003>.
- Hermelin, J.O.R., 1992. Variations in the benthic foraminiferal fauna of the Arabian Sea: a response to changes in upwelling intensity? *Geol. Soc. Lond., Spec. Publ.* 64, 151–166. <http://dx.doi.org/10.1144/GSL.SP.1992.064.01.10>.
- Hernández-Molina, F.J., et al., 2014. Onset of Mediterranean outflow into the North Atlantic. *Science* 344, 1244–1250. <http://dx.doi.org/10.1126/science.1251306>.
- Huang, Y., Clemens, S.C., Liu, W., Wang, L., Prell, W.L., 2007. Large-scale hydrological change drove the late Miocene C4 plant expansion in the Himalayan foreland and Arabian peninsula. *Geology* 35, 531–534.
- Johnson, G.C., Warren, B.A., Olson, D.B., 1991a. A deep boundary current in the Arabian Basin. *Deep-Sea Res.* 38, 653–661.
- Johnson, G.C., Warren, B.A., Olson, D.B., 1991b. Flow of bottom water in the Somali Basin. *Deep-Sea Res.* 38, 637–652.
- Juan, C., Ercilla, G., Hernández-Molina, F.J., Estrada, F., Alonso, B., Casas, D., García, M., Farran, M.L., Llave, E., Palomino, D., Vázquez, J.-T., Medialdea, T., Gorini, C., d’Acremont, E., El Moumni, B., Ammar, A., CONTOURIBER, MONTERA and MOWER Teams, 2016. A new stratigraphy and depositional model for the Pliocene and quaternary Alboran Basin. Implications for the paleoceanography. *Mar. Geol.* 378, 292–311.
- Karas, C., Nürnberg, D., Gupta, A.K., Tiedemann, R., Mohan, K., Bickert, T., 2009. Mid Pliocene climate change amplified by a switch in Indonesian subsurface throughflow. *Nat. Geosci.* 2, 434–438.
- Kolla, V., Moore, D.G., Curran, J.R., 1976. Recent bottom-current activity in the deep western bay of Bengal. *Mar. Geol.* 21, 255–270.
- Kroon, D., Steens, T., Troelstra, S.R., 1991. Onset of Monsoonal Related Upwelling in the Western Arabian Sea as Revealed by Planktonic Foraminifers. In: Prell, W.L., Niitsuma, N., et al. (Eds.), *Proceedings of the Ocean Drilling Project, Sci. Results vol.117*. College Station, Texas, pp. 257–263 (Ocean Drilling Program).
- Le Houedec, S., Meynadier, L.M., Allègre, C.J., 2012. Nd isotope systematics on ODP sites 756 and 762 sediments reveal major volcanic, oceanic and climatic changes in South Indian Ocean over the last 35 Ma. *Earth Planet. Sci. Lett.* 327–328, 29–38. <http://dx.doi.org/10.1016/j.epsl.2012.01.019>.

- Lozier, M.S., 2010. Deconstructing the conveyor belt. *Science* 328, 1507–1511.
- Lüdmann, T., Kalvelage, C., Betzler, C., Fürstenau, J., Hübscher, C., 2013. The Maldives, a giant isolated carbonate platform dominated by bottom currents. *Mar. Pet. Geol.* 43, 326–340. <http://dx.doi.org/10.1016/j.marpetgeo.2013.01.004>.
- Marlow, J.R., Lange, C.B., Wefer, G., Rosell-Melé, A., 2000. Upwelling intensification as part of the Pliocene-Pleistocene climate transition. *Science* 290, 2288–2291. <http://dx.doi.org/10.1126/science.290.5500.2288>.
- Merkouriev, S., DeMets, C., 2006. Constraints on Indian plate motion since 20 Ma from dense Russian magnetic data: implications for Indian plate dynamics. *Geochem. Geophys. Geosyst.* 7, Q02002. <http://dx.doi.org/10.1029/2005GC001079>.
- Miller, K.G., Mountain, G.S., Wright, J.D., Browning, J.V., 2011. A 180-million-year record of sea level and ice volume variations from continental margin and deep-sea isotopic records. *Oceanography* 24, 40–53. <http://dx.doi.org/10.5670/oceanog.2011.26>.
- Molnar, P., 2005. Mio-Pliocene growth of the Tibetan plateau and evolution of east Asian climate. *Palaeontol. Electron.* 8, 1–23.
- Molnar, P., 2008. Closing of the central American seaway and the ice age: a critical review. *Paleoceanography* 23, PA2201. <http://dx.doi.org/10.1029/2007PA001574>.
- Molnar, P., Boos, W.R., Battisti, D.S., 2010. Orographic controls on climate and paleoclimate of Asia: thermal and mechanical role of the Tibetan plateau. *Annu. Rev. Earth Planet. Sci.* 38, 77–102.
- Montes, C., Cardona, A., Jaramillo, C., Pardo, A., Silva, J.C., Valencia, V., Ayala, C., Pérez-Angel, L.C., Rodríguez-Parra, L.A., Ramirez, V., Niño, H., 2015. Middle Miocene closure of the central American seaway. *Science* 348, 226–229. <http://dx.doi.org/10.1126/science.1252815>.
- Morrison, J.M., 1997. Inter-monsoonal changes in the T-S properties of the near-surface waters of the northern Arabian Sea. *Geophys. Res. Lett.* 24, 2553–2556.
- Morrison, J.M., 1998. In Report of the Indian Ocean Synthesis Group on the Arabian Sea Process Study. Joint Global Ocean Flux Study Report Vol. 35 pp. 9–12.
- Mountain, G.S., Prell, W.L., 1990. A Multiphase Plate Tectonic History of the Southeast Continental Margin of Oman. In: Robertson, A.H.F., Searle, M.P., Ries, A.C. (Eds.), *The Geology and Tectonics of the Oman Region*. Geological Society (London) Special Publications Vol. 49, pp. 725–743.
- Muraleedharan, P.S., Kumar, S.P., 1996. Arabian Sea upwelling - a comparison between coastal and open ocean regions. *Curr. Sci.* 71, 842–846.
- Niemi, T.M., Ben-Avraham, Z., Hartnady, C.J.H., Reznikov, M., 2000. Post-Eocene seismic stratigraphy of the deep ocean basin adjacent to the southeast African continental margin: a record of geostrophic bottom current systems. *Mar. Geol.* 162, 237–258.
- Philander, S.G., Fedorov, A.V., 2003. Role of tropics in changing the response to Milankovich forcing some three million years ago. *Paleoceanography* 18, 1045. <http://dx.doi.org/10.1029/2002PA000837>.
- Poore, H.R., Samworth, R., White, N.J., Jones, S.M., McCave, I.N., 2006. Neogene overflow of northern component water at the Greenland Scotland ridge. *Geochem. Geophys. Geosyst.* 7, Q06010. <http://dx.doi.org/10.1029/2005GC001085>.
- Preu, B., Spieß, V., Schwenk, T., Schneider, R., 2011. Evidence for current-controlled sedimentation along the southern Mozambique continental margin since early Miocene times. *Geo-Mar. Lett.* 31, 427–435. <http://dx.doi.org/10.1007/s00367-011-0238-y>.
- Quade, J., Cerling, T.E., Bowman, J.R., 1989. Development of Asian monsoon revealed by marked ecological shift during the latest Miocene in northern Pakistan. *Nature* 342, 163–166.
- Rebesco, M., Hernández-Molina, F.J., Van Rooij, D., Wahlin, A., 2014. Contourites and associated sediments controlled by deep-water circulation processes: state of the art and future considerations. *Mar. Geol.* 352, 111–154.
- Reed, D.L., Meyer, A.W., Silver, E.A., Prasetyo, H., 1987. Contourite sedimentation in an intraoceanic forearc system: eastern Sunda Arc, Indonesia. *Mar. Geol.* 76, 223–241.
- Reid, J.L., 2003. On the total geostrophic circulation of the Indian Ocean: flow patterns, tracers, and transports. *Prog. Oceanogr.* 56, 137–186.
- Rodríguez, M., 2013. La Limite de Plaque Inde-Arabie: évolution Structurale Du Crétacé supérieur à l'Actuel et aléa Tsunami associé (Phd thesis; 403 pp.) Univ. Paris VI, France.
- Rodríguez, M., Fournier, M., Chamot-Rooke, N., Huchon, P., Bourget, J., Sorbier, M., Zaragosi, S., Rabaut, A., 2011. Neotectonics of the Owen fracture zone (NW Indian Ocean): structural evolution of an oceanic strike-slip plate boundary. *Geochem. Geophys. Geosyst.* 12. <http://dx.doi.org/10.1029/2011GC003731>.
- Rodríguez, M., Chamot-Rooke, N., Fournier, M., Huchon, P., Delescluse, M., 2013. Mode of opening of an intra-oceanic pull-apart: the 20°N Basin along the Owen Fracture Zone (NW Indian Ocean). *Tectonics* 32, 1–15. <http://dx.doi.org/10.1002/tect.20083>.
- Rodríguez, M., Chamot-Rooke, N., Huchon, P., Fournier, M., Delescluse, M., 2014a. The Owen ridge uplift in the Arabian Sea: implications for the sedimentary record of Indian monsoon in late Miocene. *Earth Planet. Sci. Lett.* 394, 1–12. <http://dx.doi.org/10.1016/j.epsl.2014.03.011>.
- Rodríguez, M., Chamot-Rooke, N., Huchon, P., Fournier, M., Lallemand, S., Zaragosi, S., Delescluse, M., Mouchot, N., 2014b. Tectonics of the Dalrymple trough and uplift of the Murray ridge (NW Indian Ocean). *Tectonophysics* 636, 1–17.
- Rodríguez, M., Huchon, P., Chamot-Rooke, N., Fournier, M., Delescluse, M., 2016. Tracking the Paleogene India-Arabia plate boundary. *Mar. Pet. Geol.* 72, 336–358. <http://dx.doi.org/10.1016/j.marpetgeo.2016.02.019>.
- Sanyal, P., Sinha, R., 2010. Evolution of the Indian Summer Monsoon: Synthesis of Continental Records. In: Clift, P.D., Tada, R., Zheng, H. (Eds.), *Monsoon Evolution and Tectonics—Climate Linkage in Asia*. Geological Society (London) Special Publications Vol. 342, pp. 153–183.
- Sanyal, P., Sarkar, A., Bhattacharya, S.K., Kumar, R., Ghosh, S.K., Agrawal, S., 2010. Intensification of monsoon, microclimate and asynchronous C4 appearance: isotopic evidence from the Indian Siwaliks sediments. *Palaeogeogr. Palaeoclimatol. Palaeoecol.* 296, 165–173.
- Schott, F.A., McCreary Jr., J.P., 2001. The monsoon circulation of the Indian Ocean. *Prog. Oceanogr.* 51, 1–123.
- Schott, F.A., Dengler, M., Schoenfeldt, R., 2002. The shallow overturning circulation of the Indian Ocean. *Prog. Oceanogr.* 53, 57–103.
- Séranne, M., Abeigne, C.-R.N., 1999. Oligocene to Holocene sediment drifts and bottom currents on the slope of Gabon continental margin (West Africa). Consequences for sedimentation and southeast Atlantic upwelling. *Sediment. Geol.* 128, 179–199.
- Seton, M., Müller, R.D., Zahirovic, S., Gai, C., Torsvik, T., Shepard, G., Talsma, A., Gurnis, M., Turner, M., Maus, S., Chandler, M., 2012. Global continental and ocean basin reconstructions since 200 Ma. *Earth-Sci. Rev.* 113, 212–270. <http://dx.doi.org/10.1016/j.earscirev.2012.03.002>.
- Shi, W., Morrison, J.M., Böhm, E., Manghni, V., 1999. Remotely sensed features in the US JGOFs Arabian Sea process study. *Deep-Sea Res.* II 46, 1551–1575.
- Shi, W., Morrison, J.M., Böhm, E., Manghni, V., 2000. The Oman upwelling zone during 1993, 1994 and 1995. *Deep-Sea Res.* II 47, 1227–1247.
- Shillington, D.J., Seeber, L., Sorlien, C.C., Steckler, M.S., Kurt, H., Dondurur, D., Çifçi, G., İmren, C., Cormier, M.H., McHugh, C.M.G., Gürçay, S., Poyraz, D., Okay, S., Atgin, O., Diebold, J.B., 2012. Evidence of widespread creep on the flanks of the sea of Marmara transform basin from marine geophysical data. *Geology* 40, 439–442.
- Shipboard Scientific Party, 1989. Site 728. In: Prell, W.L., Niitsuma, N., et al. (Eds.), *Proc. ODP, Init. Repts. Vol. 117*. College Station, TX (Ocean Drilling Program).
- Steinke, S., Groeneveld, J., Johnstone, H., Rendle-Bühning, R., 2010. East Asian summer monsoon weakening after 7.5 Ma: evidence from combined planktonic foraminifera Mg/Ca and $\delta^{18}O$ (ODP site 1146; northern South China Sea). *Palaeogeogr. Palaeoclimatol. Palaeoecol.* 289, 33–43.
- Uenzelmann-Neben, G., Watkeys, M.K., Kretzinger, W., Frank, M., Heuer, L., 2011. Palaeoceanographic interpretation of a seismic profile from the southern Mozambique ridge, southwestern Indian Ocean. *S. Afr. J. Geol.* 114, 449–458.
- Wan, S., Clift, P.D., Li, A., Yu, Z., Li, T., Hu, D., 2012. Tectonic and climatic controls on long-term silicate weathering in Asia since 5 Ma. *Geophys. Res. Lett.* 39, L15611. <http://dx.doi.org/10.1029/2012GL052377>.
- Wiles, E., Green, A., Watkeys, M., Jokat, W., Krockner, R., 2014. A new pathway for deep water exchange between the Natal Valley and Mozambique Basin? *Geo-Mar. Lett.* 34, 525–540. <http://dx.doi.org/10.1007/s00367-014-0383-1>.
- Woodruff, F., Savin, S.M., 1989. Miocene Deepwater oceanography. *Paleoceanography* 4, 87–140.
- You, Y., 1997. Seasonal variations of thermocline circulation and ventilation in the Indian Ocean. *J. Geophys. Res.* 102, 10391–10422.
- You, Y., Tomczak, M., 1993. Thermocline circulation and ventilation in the Indian Ocean derived from water mass analysis. *Deep-Sea Res.* 40, 13–56.
- Zachos, J., Pagani, M., Sloan, L., Thomas, E., Billups, K., 2001. Trends, rhythms, and aberrations in global climate 65 Ma to present. *Science* 292, 686. <http://dx.doi.org/10.1126/science.1059412>.